AD-A185 201 AN IMPROVED COMPUTATIONAL PROCEDURE FOR THE UNSTEADY DOUBLET LATTICE METHOD(U) AERONAUTICAL RESEARCH LABS MELBOURNE (AUSTRALIA) W WALDMAN AUG 86 ARL-STRUC-R-423 1/1

UNCLASSIFIED F/G 20/4 NL

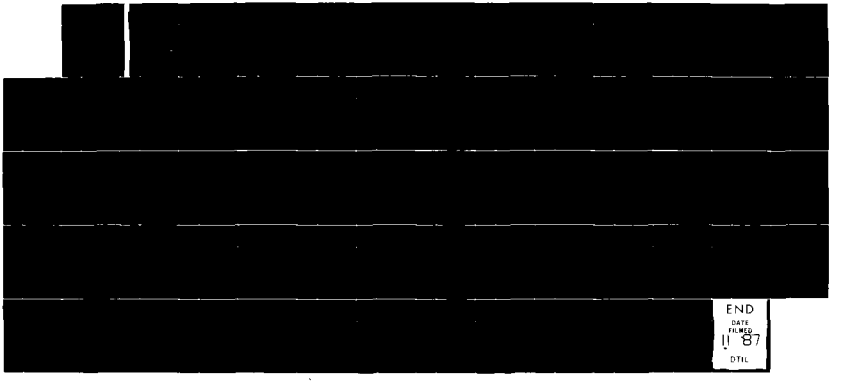

END
DATE FILMED
11 87
DTIC

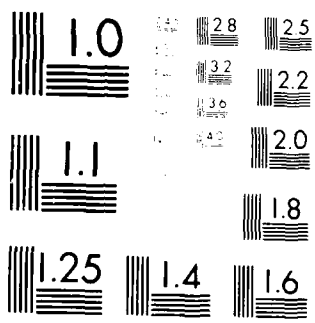

ARL-STRUC-R-423

AR-004-497

DEPARTMENT OF DEFENCE

DEFENCE SCIENCE AND TECHNOLOGY ORGANISATION

AERONAUTICAL RESEARCH LABORATORIES

MELBOURNE, VICTORIA

Structures Report 423

AN IMPROVED COMPUTATIONAL PROCEDURE FOR THE UNSTEADY DOUBLET LATTICE METHOD

by

W. Waldman

Approved for Public Release

AUGUST 1986

AR-004-497

DEPARTMENT OF DEFENCE
DEFENCE SCIENCE AND TECHNOLOGY ORGANISATION
AERONAUTICAL RESEARCH LABORATORIES

STRUCTURES REPORT 423

AN IMPROVED COMPUTATIONAL PROCEDURE FOR THE UNSTEADY DOUBLET LATTICE METHOD

by

W. WALDMAN

SUMMARY

A further modification and enhancement of the doublet lattice computational procedure in use at ARL is described. The theoretical basis for the new procedures used to integrate the unsteady Kernel function is covered in detail. A number of cases involving nonplanar and nonparallel lifting surface combinations are studied, and the results are compared with those of other workers. These show generally good agreement, although the predictions of the magnitudes of the forces acting on a tipstore and an underwing store do not compare as favourably. The present method has been implemented at ARL into the FORTRAN 77 program called DOULAT.

POSTAL ADDRESS: Director, Aeronautical Research Laboratories,
Box 4331, P.O., Melbourne, Victoria, 3001, Australia

CONTENTS

LIST OF SYMBOLS

A, B	points at either end of the doublet line on the sending panel
A_k	nondimensional area of the k'th panel defined in Equations 6·25 and 6·26
C	control point on receiving panel
$C_i^{(1)}, C_i^{(2)}$	weights used in finite part integration of the planar and nonplanar parts of the Kernel function, defined in Equations B·20 and B·21
C_M	unsteady pitching moment coefficient defined in Equation 6·26
C_{MJ}	unsteady spanwise sectional pitching moment coefficient defined in Equation 6·18
C_N	unsteady yawing moment coefficient defined in Equation 6·37
C_Y	unsteady side force coefficient defined in Equation 6·36
C_Z	unsteady normal force coefficient defined in Equation 6·25
C_{ZJ}	unsteady spanwise sectional normal force coefficient defined in Equation 6·17
c_r	root chord
$\bar{c}$	mean geometric chord of NLR wing; $\bar{c} = 0{\cdot}4183$ m
D_{rs}	element of matrix of aerodynamic normalwash influence coefficients defined in Equation 2·2
$D_{rs}^{(1)}, D_{rs}^{(2)}$	planar and nonplanar parts of D_{rs} defined in Equations 4·12 and 4·13
F	frequency of oscillation in Hz
f	nondimensional mode shape
$G^{(1)}, G^{(2)}$	numerators of the planar and nonplanar parts of the Kernel function defined in Equations A·4 and A·5
h	vertical separation between wing and tail defined in Section 6·1
i	$\sqrt{-1}$
$\mathbf{i}, \mathbf{j}, \mathbf{k}$	orthogonal unit vectors in the x, y and z directions
K	Kernel function defined in Equation 3·1
K_{rs}	Kernel function relating the induced normalwash at a receiving point r to the pressure at a sending point s

K_1, K_2	elements of the planar and nonplanar parts of the Kernel function defined in Equations 3·4 and 3·5
k	nondimensional frequency parameter, $\omega l/U$
l	reference length
l_s	quarter chord line of s'th panel defined in Equation 2·4
M	free stream Mach number
M	unsteady pitching moment defined in Equation 6·24
M_j	unsteady spanwise sectional pitching moment defined in Equation 6·16
N	unsteady yawing moment defined in Equation 6·33
n	number of straight line segments into which the interval l_s is divided
p	pressure defined in Equation 2·1
Q	generalised force coefficient
r	control point on the receiving panel located at the 3 4-chord point and illustrated in Figure 4
$\mathbf{r}_{AB}(\sigma)$	position vector of points along the doublet line of a panel as a function of non-dimensional position parameter σ defined in Equation 5·1
s	semi-span
T_1, T_2	elements of the planar and nonplanar parts of the Kernel function defined in Equations 3·2 and 3·3
T_2^*	element of the nonplanar part of the Kernel function defined in Equation 4·9
t	time
U	free stream velocity
$W_i^{(1)}$, $W_i^{(2)}$	weights used in integration of the planar and nonplanar parts of the Kernel function when $r^2 > 0$, defined in Equations A·37 and A·38
w	dimensional normalwash defined in Equation 2·1
$X_{AB}(\sigma)$, $Y_{AB}(\sigma)$, $Z_{AB}(\sigma)$	components in the **i**, **j**, **k** directions of the position vector $\mathbf{r}_{AB}(\sigma)$ defined in Equation 5·1
x, y, z	orthogonal coordinates of a point defined using the global (X, Y, Z) coordinate system of Figure 1
x_{BAL}	dimensional x-ordinate of the balance centre defined in Equations 6·26 and 6·35
x_k	dimensional x-ordinate of the lift point on the k'th panel defined in Equations 6·26 and 6·35

$\hat{x}_j$ dimensional x-ordinate of the 1/4-chord point of the j'th section defined in Equation 6·18

Y unsteady side force defined in Equation 6·32

Z unsteady normal force defined in Equations 6·23 and 6·30

α nondimensional normalwash defined in Equation 2·3

ϵ parameter used as a criterion for selecting the appropriate integration scheme, defined in Equations 5·15–5·17

β $\sqrt{1 - M^2}$

β_s sweep angle of quarter chord line of the s'th sending panel defined in Equation 2·4

γ_r, γ_s dihedral angles of the receiving and sending points defined in Equations 3·2 and 3·3

θ angular rotation in torsion

λ nondimensional pressure defined in Equation 2·5

ρ density of air in the free stream

σ parametric position coordinate defined in Equation 5·1

ω circular frequency of oscillation

Subscripts and superscripts

$^{(1)}$ denotes planar part of variable or function

$^{(2)}$ denotes nonplanar part of variable or function

$_A$ denotes value at point A on doublet line

$_B$ denotes value at point B on doublet line

$_{ij}$ denotes quantity relating to a panel in the i'th row of the j'th streamwise column of panels

$_r$ denotes receiving panel or point

$_s$ denotes sending panel or point

$^{(S)}$ denotes a quantity relating to the steady Kernel function.

1. INTRODUCTION

A previous report by Waldman [1] describes a FORTRAN program for calculating generalised air forces on arbitrary combinations of lifting surfaces. The method used therein is a variation of the doublet lattice method of Albano and Rodden [2]. This report describes further modifications and enhancements to the integration procedures used.

The initial formulation of the doublet lattice method [2] is adequate for calculating interference effects on general nonplanar lifting surface configurations; however, some computational difficulties have occurred for nearly coplanar wing/horizontal tail combinations [3, 4, 5]. The formulation of the doublet lattice method used in [1] is able to deal with nearly coplanar surfaces, up to the point where the vertical separation is so small as to be negligible. Although the method yields accurate results, it is computationally expensive, especially for nearly coplanar surfaces, since the number of integration points needed is large.

A significantly improved method for carrying out the required integrations has been developed and implemented. This uses some features of the approach proposed by Giesing *et al.* [4] and extends the techniques found in [1].

2. THE DOUBLET LATTICE METHOD

The doublet lattice method is a panel method for the solution of the oscillatory subsonic pressure-normalwash integral equation for multiple interfering surfaces

$$\frac{w(x_r, y_r, z_r)}{U} = \frac{1}{4\pi\rho U^2} \int\!\!\!\!\!\!\times_{L.S.} \int K(x_r - x_s, y_r - y_s, z_r - z_s;\ M, \omega)\, p(x_s, y_s, z_s)\, dS \qquad 2\cdot1$$

where $w(x_r, y_r, z_r)\, e^{i\omega t}$ is the induced oscillatory normalwash, $p(x_s, y_s, z_s)\, e^{i\omega t}$ is the pressure distribution over all lifting surfaces, $L.S.$, and K is the subsonic nonplanar Kernel function. The coordinates of the sending and receiving points are given by (x_s, y_s, z_s) and (x_r, y_r, z_r). The symbol $\int\!\!\!\!\!\!\times$ indicates integration in the sense of Mangler [6].

In the doublet lattice method the lifting surfaces are divided into small trapezial panels, as shown in Figure 1. By assuming that the unknown pressure p is uniform over a panel, Albano and Rodden [2] have shown that the integral equation, Equation 2·1, reduces to a set of linear simultaneous equations. These may be written in matrix form as

$$\{\alpha_r\} = [D_{rs}]\,\{\lambda_s\} \qquad 2\cdot2$$

where

$$\alpha_r = \frac{w_r(x_r, y_r, z_r)}{U} \qquad 2\cdot3$$

$$D_{rs} = \frac{c_s \cos\beta_s}{4\pi} \int\!\!\!\!\!\!\times_{l_s} K_{rs}\, dl \qquad 2\cdot4$$

$$\lambda_s = \frac{p_s(x_s, y_s, z_s)}{\rho U^2} \qquad 2\cdot5$$

c_s is the mean chord of the s'th sending panel

β_s is the sweep angle of the 1/4-chord line of the s'th sending panel

K_{rs} is the subsonic nonplanar Kernel function relating the normalwash at the control point (mid-span 3/4-chord point) on the r'th receiving panel to the pressure occurring at a sending point on the s'th sending panel

l_s denotes that the integration is carried out along the 1/4-chord line of the s'th sending panel.

By evaluating Equation 2·4 we are calculating the contribution to the normalwash at a (receiving) point on panel r that is due to the uniform pressure occurring over a (sending) panel s.

3. THE KERNEL FUNCTION

The Kernel function relates the complex normalwash $w(x_r, y_r, z_r)\, e^{i\omega t}$ to the complex pressure $p(x_s, y_s, z_s)\, e^{i\omega t}$, and can be written in the following form

$$K = e^{\frac{-i\omega x_1}{U}} (K_1 T_1 + K_2 T_2)/r^2 \qquad 3\cdot1$$

where

$$T_1 = \cos(\gamma_r - \gamma_s) \qquad 3\cdot2$$

$$T_2 = \{z_1 \cos\gamma_r - y_1 \sin\gamma_r\}\{z_1 \cos\gamma_s - y_1 \sin\gamma_s\}\, r^2 \qquad 3\cdot3$$

$$K_1 = I_1 + \frac{Mr}{R}(1 + u_1^2)^{-1/2} e^{-ivu_1} \qquad 3\cdot4$$

$$K_2 = -3I_2 - \frac{ivM^2r^2}{R^2}(1 + u_1^2)^{-1/2} e^{-ivu_1} - \frac{Mr}{R}\left[(1 + u_1^2)\frac{\beta^2 r^2}{R^2} + 2 + \frac{Mru_1}{R}\right](1 + u_1^2)^{-1/2} e^{-ivu_1} \qquad 3\cdot5$$

$$x_1 = x_r - x_s \qquad y_1 = y_r - y_s \qquad z_1 = z_r - z_s \qquad 3\cdot6$$

$$\beta = (1 - M^2)^{1/2} \qquad r = (y_1^2 + z_1^2)^{1/2} \qquad R = (x_1^2 + \beta^2 r^2)^{1/2} \qquad 3\cdot7$$

$$v = \frac{\omega r}{U} \qquad u_1 = \frac{MR - x_1}{\beta^2 r} \qquad 3\cdot8$$

and γ_r and γ_s are the dihedral angles of the receiving and sending points located at (x_r, y_r, z_r) and (x_s, y_s, z_s). The terms I_1 and I_2 represent the two infinite integrals

$$I_1(u_1, v) = \int_{u_{1a}}^{\infty} \frac{e^{-ivu}}{(1 + u^2)^{1/2}}\, du \qquad 3\cdot9$$

$$I_2(u_1, v) = \int_{u_1}^{\infty} \frac{e^{-ivu}}{(1 + u^2)^{5/2}}\, du \qquad 3\cdot10$$

Techniques for the calculation of I_1 and I_2 can be found in [1, 4].

Note that for the steady case ($\omega = 0$), the expressions for K_1 and K_2 simplify to [7]

$$K_1^{(s)} = \frac{x_1}{R} + 1 \qquad 3\cdot11$$

$$K_2^{(s)} = \left(\frac{x_1}{R} - 2\right)\left(\frac{x_1}{R} + 1\right)^2 \qquad 3\cdot12$$

In discussions involving the Kernel function it is customary and convenient to refer to the terms incorporating $K_1 T_1$ as the planar part of the function. The terms incorporating $K_2 T_2$ are referred to as the nonplanar part of the function.

4. BEHAVIOUR OF THE KERNEL FUNCTION

The general form of the nonplanar Kernel function, K, was given in Equation 3·1 as:

$$K = e^{-\frac{i\omega x_1}{U}} (K_1 T_1 + K_2 T_2)\, r^2 \qquad 4\cdot1$$

The formal basis of the doublet lattice method is to approximate the numerator of K with a polynomial and integrate Equation 2·3 analytically [2]. The integration used to obtain the normal-wash influence coefficients, D_{rs}, works well for all cases, planar and nonplanar, with the exception of the nearly coplanar case [3, 4, 5].

Consider the case where the receiving point is downstream of the sending panel, where X defines the downstream direction in Figure 1. When there exists a small normal separation between the receiving point and the plane of the sending panel, then the numerator of the Kernel function has large variations along the interval l_s in the line integral

$$D_{rs} = \frac{c_s \cos\beta_s}{4\pi} \int_{l_s} K_{rs}\, dl \qquad 4\cdot2$$

The typical behaviour of the numerator of the steady Kernel function is illustrated in Figure 2. Values of the numerator, $(K_1^{(s)} T_1 + K_2^{(s)} T_2)$, are plotted against the spanwise variable y_1 in the vicinity of $y_1 = 0$ for three values of vertical distance z_1 and a chordwise distance $x_1 = 0{\cdot}5$. Both the sending and receiving panels lie in planes parallel to the horizontal plane. Note that the curves are asymptotic to the value $(K_1^{(s)} T_1 + K_2^{(s)} T_2) = 1{\cdot}0$ for values of $y_1 = \pm z_1$, although this is not apparent from Figure 2. Giesing *et al* [4] have found that when the length l_s of the line integral is large compared with z_1 ($l_s > 3z_1$) the variations of $(K_1^{(s)} T_1 + K_2^{(s)} T_2)$ across the panel are very large. Therefore a second order polynominal fit is inadequate.

Expressions for the various parts of the unsteady Kernel function valid for small values of y_1, and downstream of the sending point are [4]

$$K_1 \to 2 \tag{4·3}$$

$$K_2 \to -4 \tag{4·4}$$

$$T_1 = \cos(\gamma_r - \gamma_s) \tag{4·5}$$

$$T_2 = (z_1 \cos\gamma_r - y_1 \sin\gamma_r)(z_1 \cos\gamma_s - y_1 \sin\gamma_s)/r^2 \tag{4·6}$$

where $r^2(= y_1^2 + z_1^2) \to 0$ and $x_1 > 0$. Using Equations 4·3 to 4·6 in the numerator gives

$$\lim_{r^2 \to 0} e^{\frac{-i\omega x_1}{U}} \{K_1 T_1 + K_2 T_2\}$$

$$= e^{\frac{-i\omega x_1}{U}} \{2\cos(\gamma_r - \gamma_s) - 4(z_1 \cos\gamma_r - y_1 \sin\gamma_r)(z_1 \cos\gamma_s - y_1 \sin\gamma_s)/r^2\} \tag{4·7}$$

The term that requires the most care during integration arises from the nonplanar term and is the one divided by r^2 and involves T_2. A plot of T_2 as a function of y_1 is given in Figure 3 for $\gamma_s = 0°$, $\gamma_r = 45°$ and two values of z_1. It is clear that a low-order polynomial fit will not give accurate results when r/l_s is small.

One solution to this problem is to consider the nonplanar terms separately from the planar. The planar terms vary as $1/r^2$ but the nonplanar terms vary as $1/r^4$, hence the Kernel function can be written as [4]

$$K = e^{\frac{-i\omega x_1}{U}} (K_1 T_1 r^2 + K_2 T_2^* r^4) \tag{4·8}$$

where

$$T_2^* = r^2 T_2 = (z_1 \cos\gamma_r - y_1 \sin\gamma_r)(z_1 \cos\gamma_s - y_1 \sin\gamma_s) \tag{4·9}$$

Equation 4·8 may be rewritten as

$$K = e^{\frac{-i\omega x_1}{U}} K_1 T_1/r^2 + e^{\frac{i\omega x_1}{U}} K_2 T_2^* r^4 \tag{4·10}$$

and the numerators of each of the terms may now be approximated with a low-order polynomial since they are slowly varying functions over the line interval l_s.

Hence, Equation 4·2 may be written as

$$D_{rs} = D_{rs}^{(1)} + D_{rs}^{(2)} \tag{4·11}$$

where

$$D_{rs}^{(1)} = \frac{c_s \cos\beta_s}{4\pi} \int_{l_s} e^{\frac{-i\omega x_1}{U}} K_1 T_1 r^2 \, dl \tag{4·12}$$

$$D_{rs}^{(2)} = \frac{c_s \cos\beta_s}{4\pi} \int_{l_s} e^{\frac{i\omega x_1}{U}} K_2 T_2^* r^4 \, dl \tag{4·13}$$

By a suitable choice of integration scheme, it is possible to analytically incorporate the $1/r^2$ and $1/r^4$ behaviour into the integration procedure. This has the effect of minimising computational errors involved in evaluating the integrals over regions where r is small or becomes equal to zero.

5. INTEGRATION OF THE KERNEL FUNCTION

5.1 Geometric Considerations

In calculating the aerodynamic influence coefficients defined by Equation 2·4, let us consider the interaction of a receiving panel r and a sending panel s, as shown in Figure 4.

The position vector corresponding to points along the doublet line may be written in terms of the parametric variable σ as follows

$$\mathbf{r}_{AB}(\sigma) = X_{AB}(\sigma)\,\mathbf{i} + Y_{AB}(\sigma)\,\mathbf{j} + Z_{AB}(\sigma)\,\mathbf{k} \quad 0 \leq \sigma \leq 1 \qquad 5\cdot1$$

where

$$X_{AB}(\sigma) = x_A + (x_B - x_A)\,\sigma \qquad 5\cdot2$$

$$Y_{AB}(\sigma) = y_A + (y_B - y_A)\,\sigma \qquad 5\cdot3$$

$$Z_{AB}(\sigma) = z_A + (z_B - z_A)\,\sigma \qquad 5\cdot4$$

From the definitions of x_1, y_1, and z_1 in Equation 3·6 it is clear that when evaluating the line integral of Equation 2·4 the variables x_1, y_1, and z_1 may be written in the following form

$$x_1 = a_x + b_x\sigma \qquad y_1 = a_y + b_y\sigma \qquad z_1 = a_z + b_z\sigma \qquad 5\cdot5$$

where

$$a_x = x_r - x_A \qquad a_y = y_r - y_A \qquad a_z = z_r - z_A \qquad 5\cdot6$$

$$b_x = x_A - x_B \qquad b_y = y_A - y_B \qquad b_z = z_A - z_B \qquad 5\cdot7$$

In the equation for the Kernel function the variable r^2 is present. The equation for r^2 may be written as

$$r^2 = a_r\sigma^2 + b_r\sigma + c_r \qquad 5\cdot8$$

where

$$a_r = b_y^2 + b_z^2 \qquad 5\cdot9$$

$$b_r = 2[a_y b_y + a_z b_z] \qquad 5\cdot10$$

$$c_r = a_y^2 + a_z^2 \qquad 5\cdot11$$

If the minimum value of r^2 for a given panel combination is denoted by r^2_{min}, and the location of this minimum by σ_{min}, then we have that

$$\sigma_{min} = \frac{-b_r}{2a_r} \qquad 5\cdot12$$

$$r^2_{min} = c_r - \frac{b_r^2}{4a_r} \qquad 5\cdot13$$

The span of a given sending panel, Δs, may be calculated from

$$\Delta s^2 = b_y^2 + b_x^2 \qquad 5\cdot14$$

Due to the organisation of panels into streamwise columns, σ_{min}, r^2_{min} and Δs need only be calculated for combinations of columns, rather than individual combinations of panels. This strategy reduces the number of times these three parameters are calculated.

5.2 Basis for Choice of Integration Procedure

A decision which determines the integration procedure to be used is made on the basis of the values r_{min}, σ_{min} and Δs that have been calculated for a given combination of sending and receiving columns of panels. One of the following conditions can occur for such a combination

$$\text{(i)}\ r_{min}/\Delta s > \epsilon \qquad -\infty > \sigma_{min} > +\infty \qquad 5\cdot15$$

$$\text{(ii)}\ 0 \leq r_{min}/\Delta s \leq \epsilon \qquad \sigma_{min} < 0 \text{ or } \sigma_{min} > 1 \qquad 5\cdot16$$

$$\text{(iii)}\ 0 \leq r_{min}/\Delta s \leq \epsilon \qquad 0 \leq \sigma_{min} \leq 1 \qquad 5\cdot17$$

where ϵ is some small number (typically, $\epsilon = 0\cdot01$ in the program). The ratio $r_{min}/\Delta s$ is a non-dimensional parameter that compares the smallest value of r obtained for a given combination of sending and receiving panels with the span of the sending column of panels. For computational purposes, the singularity $r = 0$ is assumed to occur when r_{min} lies in the range defined by $0 \leq r_{min}/\Delta s \leq \epsilon$.

Condition (i) corresponds to the case where no singularity occurs for the combination of sending and receiving panels (or columns) being considered. The integration procedure used is described in Appendix A for the case where the interval l_s is subdivided into n smaller subintervals. In the program the integration for condition (i) is evaluated with $n = 1$.

Condition (ii) corresponds to the case where a singularity occurs, but it lies outside the interval of integration l_s. The integration procedure described in Appendix A is applied with $n = 1$.

Condition (iii) corresponds to the case where the singularity occurs within the interval of integration l_s. The singularity is assumed to occur in the centre of the interval. This requirement can be met by aligning all columns of panels in streamwise strips. The integration procedure used is described in Appendix B for the case where the interval l_s is subdivided into $(2n - 1)$ straight line segments. In the program $n = 4$ and the singularity falls in the centre of the 4th subinterval. The width of the fourth subinterval is l_s/n. The remaining six subintervals are placed symmetrically about the segment containing the singularity, three on either side, and the length of each of these subintervals is $l_s/(2n)$. The choice of $n = 4$ follows the technique used by Farrell [5]. By changing a PARAMETER statement in the FORTRAN source code (IR2EQ0 $= 2n$, $n = 1, 2, \ldots$) it is possible to vary the integration scheme used to deal with the singularity.

In order to ensure that a high degree of numerical accuracy is maintained in all cases, it is necessary to choose an appropriate value of the parameter ϵ, used previously in Equations 5·15 to 5·17. If the chosen value of ϵ is too large then the "finite part" integration techniques of Appendix B will be applied when there is no singularity present. On the other hand, if ϵ is too small then the proximity effects of the approaching singularity will cause the integration techniques of Appendix A to lose numerical accuracy.

Giesing *et al.* [4] have investigated this situation. They found that numerical difficulties arose in their integration algorithm when $r_{min}/\Delta s = 0\cdot00125$. With the present method, no numerical difficulties were encountered for cases with $r_{min}/\Delta s = 0\cdot01$. Hence, the value of ϵ was set at $\epsilon = 0\cdot01$, this being more conservative than the equivalent value used by Giesing *et al.* [4]. Since Δs is small, $r_{min} = \Delta s\epsilon$ is very small and can be assumed to be zero; i.e. the planar case. The small value of ϵ ensures that the transition from the case of very nearly coplanar surfaces to the case of coplanar surfaces is achieved without a discontinuity in the results.

6. COMPARISON WITH OTHER METHODS

The method described above has been implemented at ARL into the FORTRAN 77 program DOULAT. The format of the input data to DOULAT, and the definition of pressures and generalised forces, is the same as that used in [1].

In order to test and verify the operation of the present method, a number of lifting surface configurations have been investigated. The test problems selected cover a wide range of frequency parameters, Mach numbers and variations in geometry. These are designed to test both the planar and nonplanar aspects of the computational procedure, since both have been significantly modified.

The various configurations are described in Sections 6·1 to 6·5, and the comparisons of the results with those of other workers are shown in Tables 1 to 7. The comparisons include results obtained by a variety of computational formulations of the doublet lattice method, lifting surface methods, and also some experimental results.

In the Tables the results are presented in terms of modulus and phase. Where the frequency parameter is zero ($k = 0$), the steady state Kernel function was used.

6.1 AGARD Horizontal Wing and Tailplane

The AGARD horizontal wing and tail combination has been specified by AGARD for the calculation of generalised airforces. The configuration is shown in Figure 5. Calculations have been made for two values of frequency parameter, $k = 0$ and $k = 1{\cdot}5$, at Mach number $M = 0{\cdot}8$. The modes of oscillation are anti-symmetric and are defined by

$$f_1(x, y, z) = y(x - 2{\cdot}25\,y - 0{\cdot}85) \quad \text{on the wing} \qquad 6{\cdot}1$$

$$= y \quad \text{on the tail} \qquad 6{\cdot}2$$

$$f_2(x, y, z) = y\,y \quad \text{on the wing} \qquad 6{\cdot}3$$

$$= (x - 3{\cdot}35)\,\mathrm{sgn}(y) \quad \text{on the tail} \qquad 6{\cdot}4$$

where the origin of the coordinates is at the apex of the wing. The first mode is torsion of the wing about an axis 38% of the local chord, coupled with roll of the tail. The second is parabolic bending of the wing coupled with pitch of the tail.

A number of variations have been investigated for $h = 0{\cdot}0$, $0{\cdot}01$, $0{\cdot}04$, $0{\cdot}1$, $0{\cdot}2$, $0{\cdot}3$, $0{\cdot}4$, $0{\cdot}5$ and $0{\cdot}6$. Tables 1 to 3 compare the results obtained by different workers [2, 5, 8, 9, 10] with those calculated using the present method. The results of Davies [8] and Albano, Perkinson and Rodden [9] are based on lifting surface methods, and the remainder are based on various computational formulations of the doublet lattice method.

Using the present method generalised forces have been calculated for two different panel distributions. Panel distribution (1) consisted of 8 evenly spaced panels along the semi-span and 6 evenly spaced panels along the chord of the wing, and of 8 panels along the semi-span and 4 panels along the chord of the tailplane, also evenly spaced. This distribution was the same as that used by Albano and Rodden [2]. Panel distribution (2) had 8 evenly spaced panels along the chord of the wing and tailplane. All panels on the wing and tailplane are aligned in streamwise strips.

Table 1 presents generalised forces obtained for two values of frequency parameter, $k = 0$ and $k = 1{\cdot}5$, for the coplanar case. The results of the present method agree well with those of other workers. Note that the results of Farrell's doublet lattice calculations were obtained using an array of 10 panels along the semi-span and 5 panels along the chord of the wing and the tailplane.

It is worth noting that in order to converge to Hedman's [11] vortex lattice results for steady flow, and to improve the approximation of Equation 2·4, Albano and Rodden found it necessary to subtract the steady part ($k = 0$) from the Kernel function K before applying their integration formula, and then to add the effect of a horseshoe vortex which was calculated analytically. When comparing the results of the present method (1) with those of Albano and Rodden (the panel distributions for these two cases being identical) for the steady planar case ($k = 0$, $h = 0$),

it is evident that there is excellent agreement. There is also negligible difference between the results of panel distribution (1) and (2).

When comparing the results of the present method for $k = 1{\cdot}5$ and $h = 0$ with those of the refined doublet lattice method of Giesing, Kalman and Rodden, it is seen that results obtained with the finer panel distribution of the present method (2) are in excellent agreement. The results of the present method (1) do not display such good agreement, although they differ by a maximum of less than 7%.

It is interesting to note that for the unsteady case there is always excellent agreement in the phase angle calculated by the four formulations of the doublet lattice method for any given generalised force. The small variation that is evident is very much less than that occurring in the magnitudes of the generalised forces. It is also evident that the variation in results obtained using the present method and panel distributions (1) and (2) is much greater for the unsteady case than it is for the steady case.

Table 2 presents results for generalised airforces calculated with $h = 0{\cdot}6$ for $k = 0$ and $k = 1{\cdot}5$. The results of the present method once again agree well with those of other workers.

Table 3 gives a comparison of Davies lifting surface results for $k = 1{\cdot}5$ and $h = 0$ to $h = 0{\cdot}6$ with results from the present method obtained using panel distribution (2). There is good agreement in the trends predicted for the generalised airforces as the vertical separation is varied, together with an acceptable agreement between individual pairs of generalised forces. As described in Section 4, early formulations of the doublet lattice method experienced difficulties with non-planar wing and tailplane combinations where the vertical separation, h, was small [3, 4]. In the critical region of interest when $h = 0{\cdot}01$ and $h = 0{\cdot}04$ there is acceptable agreement between the results due to Davies and those of the present method. No numerical difficulties were encountered when the above two h values were used.

6.2 Stark's Swept and Tapered T-Tail

The swept and tapered T-tail analysed by Stark [12] is shown in Figure 6. For this T-tail the trailing edge of the stabiliser extends beyond the fin trailing edge at the stabiliser – fin junction. The T-tail is assumed to be oscillating in three rigid-body modes. These consist of yawing about a vertical axis through the centre of the root chord of the fin (positive nose right), sideway (positive left) and rolling about the fin-stabiliser intersection (positive right stabiliser down). These modes are defined as

$$f_1(x, y, z) = 3(x + 0{\cdot}15577) \quad \text{on the fin} \qquad 6{\cdot}5$$
$$= 0 \quad \text{on the stabiliser} \qquad 6{\cdot}6$$

$$f_2(x, y, z) = 1{\cdot}0 \quad \text{on the fin} \qquad 6{\cdot}7$$
$$= 0{\cdot}0 \quad \text{on the stabiliser} \qquad 6{\cdot}8$$

$$f_3(x, y, z) = -z \quad \text{on the fin} \qquad 6{\cdot}9$$
$$= y \quad \text{on the stabiliser} \qquad 6{\cdot}10$$

Figure 7 shows the panel distributions used on the fin and stabiliser. The present idealisation is similar to that used by Kalman, Rodden and Giesing [10].

Table 4 presents generalised airforces calculated for $k = 0$ and $M = 0$ and $M = 0{\cdot}8$. The results of the present method agree well with those of other workers. When comparing the results due to Kalman, Rodden and Giesing [10] with those of the present method, the largest difference in the generalised forces occurs for the Q_{11} term. This term represents the fin yawing moment due to yaw, and since the side force acting on the fin, Q_{21}, agrees well, this indicates that the predicted chordwise location of the centre of pressure will differ. A similar effect occurs for the Q_{11} term in the results presented for $k = 0{\cdot}6$ and $k = 0{\cdot}9$ in Table 5.

Table 5 presents generalised airforces calculated for $M = 0{\cdot}8$ and $k = 0{\cdot}6$ and $k = 0{\cdot}9$. The results due to (i) Davies, (ii) Zwaan, and (iii) Kalman, Rodden and Giesing, were obtained from [10].

The results shown in Table 5 compare favourably with those predicted by the other methods; however, the agreement between the magnitudes of the generalised forces Q_{11}, Q_{12} and Q_{13} as calculated by Farrell is comparatively poor.

The generalised forces Q_{11}, Q_{12} and Q_{13} represent the yawing moment due to yaw, sideslway and roll, respectively. Nine and eleven panels were used down the chord of the fin and stabiliser in the present method, compared with only four panels down the chord of each surface for the results due to Farrell, whilst the spanwise distributions were similar. Since the present method has a significantly finer chordwise panel distribution, it is to be expected that the yawing moments will be predicted with greater accuracy. As shown in [1], if the chordwise panel distribution is chosen to approximate more closely that used by Farrell, then the results of estimates for Q_{11}, Q_{12} and Q_{13} approach those obtained by Farrell. Note that this trend is also followed by the remaining six generalised forces.

6.3 NLR Clean Wing

This wing (Fig. 8) represents that of the *F*-5 aircraft and it has been the subject of both theoretical analysis and wind tunnel testing at the National Aerospace Laboratory (NLR) in the Netherlands [Ref. 13, Part II]. During the wind tunnel tests the model was oscillated in pitch about an axis parallel to the y-axis and passing through the mid-point of the root chord.

Two combinations of Mach number and frequency were investigated. These are $M = 0{\cdot}6$ and $F = 20$ Hz and also $M = 0{\cdot}6$ and $F = 40$ Hz. The nondimensional in-wind vibration modes are respectively [Ref. 13, Part II]

$$f_1(x, y) = (0{\cdot}330 - 1{\cdot}001x + 0{\cdot}002y - 0{\cdot}013xy + 0{\cdot}052y^2 - 0{\cdot}067xy^2)\ / \qquad 6{\cdot}11$$

$$f_2(x, y) = (0{\cdot}312 - 0{\cdot}954x - 0{\cdot}148y + 0{\cdot}532xy - 0{\cdot}339y^2 + 0{\cdot}602xy^2)\ / \qquad 6{\cdot}12$$

where the reference length, l, is taken to be equal to the root chord ($l = 0{\cdot}639$ m). Note that in Equations 6·11 and 6·12 the x- and y-ordinates must be given in metres. The expressions for f_1 and f_2 assume that there is no elastic deformation in the chordwise direction. A parabolic deformation is assumed to occur in the spanwise direction. The major component of both modes is due to rigid body pitch (rotation) about an axis through the centre of the root chord, with only a small proportion being due to a spanwise bending and torsion contribution.

The in-wind vibration modes for the clean wing are illustrated in Figure 9. The normalisation of the modes is carried out such that at the chordwise wing section containing the point $(x, y) = (0{\cdot}5648, -0{\cdot}0977)$ the chordwise slopes of the oscillatory modes are given by

$$\frac{d}{dx}(lf_1) = -1 \qquad 6{\cdot}13$$

$$\frac{d}{dx}(lf_2) = -1 \qquad 6{\cdot}14$$

Note that the displacements f_1 and f_2 are positive in the positive z-direction.

The panel distribution used in the present method (Fig. 10) is the same as that used by NLR [Ref. 13, Part II]. The present method was used to calculate the unsteady spanwise normal force and pitching moment distributions. The sectional normal force and pitching moment are given by

$$Z_j = \frac{\pi}{2}\rho V^2 c_j C_{Z_j} 0\, e^{i\omega t} \qquad 6{\cdot}15$$

$$M_j = \frac{\pi}{4}\rho V^2 c_j^2 C_{M_j} 0\, e^{i\omega t} \qquad 6{\cdot}16$$

where Z_j is positive in the positive z-direction and M_j is the pitching moment about the quarter-chord point of the section (positive nose down). The chord c_j is the local chord of the section. The sectional normal force and pitching moment coefficients are given by

$$C_{Zj} = \frac{2l^2}{\pi\, c_j\, dy_j} \sum_i \lambda_{ij}\, A_{ij} \qquad 6\cdot17$$

$$C_{Mj} = \frac{4l^3}{\pi c_j^2 dy_j} \sum_i \lambda_{ij}\, A_{ij}\, (x_{ij} - \hat{x}_j)/l \qquad 6\cdot18$$

where λ_{ij} is the nondimensional pressure acting on a panel in the i'th row of the j'th section;

$l^2 A_{ij}$ is the area of the panel in the i'th row of the j'th section;

x_{ij} is the dimensional x-ordinate of the mid-span quarter-chord point of the panel in the i'th row of the j'th section;

$\hat{x}_j$ is the dimensional x-ordinate of the quarter-chord point of the j'th section;

dy_j is the dimensional width of the panels that comprise the j'th section;

and the summation $\sum_i$ is carried out over the i panels down the chord of the j'th section.

Figures 11 to 14 show the unsteady normal force and pitching moment distributions for the clean wing obtained by the present method and compare them with results of NLR doublet lattice calculations and experimental measurements. The results of the present method are in excellent agreement with the results of NLR. Both methods predict forces that are greater than those obtained from NLR experiments.

6.4 NLR Wing with Tipstore

This configuration was studied theoretically and experimentally at NLR [Ref. 13, Part III]. It comprises a tip store added to the clean wing described in the previous section. The store represents an AIM-9J missile and launcher. The panel distribution used (Fig. 15) was chosen to conform as closely as possible to the panel distribution presented in [Ref. 13, Part III].

The nondimensional in-wind vibration modes are as follows [Ref. 13, Part III]

$$\begin{aligned} f_1(x, y) &= (0\cdot336 - 0\cdot997x + 0\cdot045y + 0\cdot032xy \\ &\quad + 0\cdot141y^2 + 0\cdot001xy^2)\,/ \qquad \text{(on wing)} \\ &= (0\cdot389 - 1\cdot022x)\,/ \qquad \text{(on store)} \end{aligned} \qquad 6\cdot19$$

$$\begin{aligned} f_2(x, y) &= (0\cdot351 - 1\cdot022x + 0\cdot162y - 0\cdot296xy \\ &\quad + 0\cdot531y^2 - 0\cdot0677y^2)\,/ \qquad \text{(on wing)} \\ &= (0\cdot459 - 1\cdot075x)\,/ \qquad \text{(on store)} \end{aligned} \qquad 6\cdot20$$

where the reference length l is taken to be equal to the root chord ($l = 0\cdot639$ m). Mode f_1 corresponds to $M = 0\cdot6$ and $F = 20$ Hz, and mode f_2 corresponds to $M = 0\cdot8$ and $F = 20$ Hz. Note that the x- and y-ordinates are to be given in metres and the term "on store" (used in Equations 6·19 and 6·20) refers to the complete store and launcher assembly.

The expressions for f_1 and f_2 assume a parabolic deformation in the spanwise direction and no elastic deformation in the chordwise direction. The major component of both modes is due to rigid body pitch (rotation) about an axis through the centre of the root chord, and a small proportion is due to spanwise bending and torsion. The displacements f_1 and f_2 are positive in the positive z-direction.

The modes are normalised such that at the chordwise wing section containing the point $(x, y) = (0{\cdot}5648, -0{\cdot}0977)$ the slopes of the oscillatory modes are given by

$$\frac{d}{dx}(lf_1) = -1 \qquad 6{\cdot}21$$

$$\frac{d}{dx}(lf_2) = -1 \qquad 6{\cdot}22$$

The nodal lines for the in-wind vibration modes for the NLR wing with tipstore are presented in Figure 16. The figure shows that as the Mach number is increased from $M = 0{\cdot}6$ to $M = 0{\cdot}8$ the nodal line is bent further rearwards. Comparing Figure 16a with Figure 9a indicates that the wing with tipstore possesses a nodal line that is bent further rearwards, especially over the outer part of the wing.

The present method has been used to calculate the unsteady spanwise normal force distribution on the wing in the presence of aerodynamic interference from the tipstore. The normal force is defined in Equation 6·17. Figure 17 compares the unsteady local normal force distribution calculated by the present method with that obtained by NLR doublet lattice calculations and experiment [Ref. 13, Part III]. It is seen that the present method agrees very well with the NLR doublet lattice results. When compared with theory, the experimental results yield smaller values for the real part of C_{Z_j} (especially near the wing tip) and larger values for the imaginary part of C_{Z_j}. This corresponds to a reduction in the magnitude of the force together with a phase shift. A comparison of Figures 11 and 17 indicates that the tipstore acts as an endplate, thus increasing the load on the wing.

The normal force coefficient C_Z and pitching moment coefficient C_M have been calculated for the tipstore (together with its launcher) using the present method. The normal force and pitching moment about the balance centre (positive nose up) are defined by the following equations

$$Z = \frac{\pi}{2}\rho V^2 \bar{c} s\, C_Z\, \theta\, e^{i\omega t} \qquad 6{\cdot}23$$

$$M = \frac{\pi}{4}\rho V^2 \bar{c}^2 s\, C_M\, \theta\, e^{i\omega t} \qquad 6{\cdot}24$$

where $\bar{c}$ is the mean geometric chord ($\bar{c} = 0{\cdot}4183$) and s is the semi span ($s = 0{\cdot}6226$). The normal force and pitching moment coefficients are given by

$$C_Z = \frac{2l^2}{\pi \bar{c} s} \sum_k \lambda_k \cos\gamma_k A_k \qquad 6{\cdot}25$$

$$C_M = -\frac{4l^3}{\pi \bar{c}^2 s} \sum_k \lambda_k \cos\gamma_k A_k (x_k - x_{BAL}) \qquad 6{\cdot}26$$

where λ_k is the nondimensional pressure on the k'th panel;

γ_k is the dihedral angle of the k'th panel;

x_k is the dimensional x-ordinate of the mid-span quarter-chord point on the k'th panel;

x_{BAL} is the dimensional x-ordinate of the balance centre ($x_{BAL} = 0{\cdot}480$ m);

$l^2 A_k$ is the dimensional area of the k'th panel;

and the summation is taken over all panels on the tipstore and launcher assembly.

Table 6 presents the unsteady normal force and pitching moment coefficients obtained by the present method and compares them with theoretical and experimental results obtained by Tijdeman *et al.* [Ref. 13, Part III]. The coefficients have been calculated for a frequency of oscillation $F = 20$ Hz and two Mach numbers, $M = 0{\cdot}6$ and $M = 0{\cdot}8$. When compared with the NLR doublet lattice method, the present method yields coefficients whose magnitudes are 11% to 31% greater, the largest variations occuring in the moment coefficients. However, in contrast to this, the agreement exhibited for the phase angles is excellent, the differences being less than $1{\cdot}1°$.

For the spanwise normal load distribution, excellent agreement has been obtained between the present method and the NLR doublet lattice method. Even at the wing tip, where the non-planar effects of the tipstore are greatest, the agreement is still very good. However, when the unsteady force and moment coefficients for the tipstore are compared, it is found that the force and moment coefficients are consistently larger when predicted by the present method. On average, the force coefficient C_Z is 13% greater, and the moment coefficient C_M is 28% greater, the differences in phase angles being negligible.

When the theoretical force and moment distributions over the wing are compared with experimental results, it is evident that the theoretical methods overestimate the magnitudes of these forces. This feature was also apparent for results for the clean wing, described in Section 6·3. However, it is not possible to isolate a similar trend in the force coefficients calculated for the tipstore.

The reader is referred to Section 7 for additional comments related to the differences between the theoretical calculations of the present method and the NLR doublet lattice method.

6.5 NLR Wing with Underwing Store

This configuration investigated by NLR [Ref. 13, Part IV] involves the addition of a pylon, launcher and missile to the clean wing described in Section 6·3. The store represents an AIM-9J missile, and is represented by additional thin lifting surfaces. The panel distribution is shown in Figure 18 and conforms as closely as possible to the panel distribution presented in [Ref. 13, Part IV].

The wing model was oscillated in pitch about a 50% root chord axis at a Mach number $M = 0{\cdot}6$ and frequency $F = 20$ Hz. The resulting vibration mode on the store consisted of both vertical and lateral motion. The nondimensional in-wind vibration mode is defined as [Ref. 13, Part IV]

$$f_V(x, y) = \begin{cases} (0{\cdot}302 - 0{\cdot}891x - 0{\cdot}362y + 1{\cdot}371xy \\ \quad -0{\cdot}681y^2 + 2{\cdot}606(xy^2))/ & \text{(on wing)} \\ (0{\cdot}320 - 0{\cdot}952x)/ & \text{(on store)} \end{cases} \qquad 6{\cdot}27$$

$$f_L(x, y) = \begin{cases} 0{\cdot}0 & \text{(on wing)} \\ (-0{\cdot}017 + 0{\cdot}047x)/ & \text{(on store)} \end{cases} \qquad 6{\cdot}28$$

where the term "on store" refers to the store, pylon and launcher assembly. The vertical component of the modal displacement is given by f_V, for which the displacements are positive in the positive z-direction. The lateral component of the mode is given by f_L, for which the displacements are positive in the positive y-direction. The reference length $l = 0{\cdot}6396$ m and the x- and y-ordinates are assumed to be given in metres.

The expression for f_V on the wing assumes a parabolic deformation in the spanwise direction and no elastic deformation in the chordwise direction. The major component of f_V is due to rigid body pitch (rotation) about an axis through the centre of the root chord, with a small contribution being due to a spanwise bending and torsion distribution. The lateral component of the displacement mode, f_L, is composed of rigid body yaw and sideway of the underwing store assembly.

The mode is normalised such that at the chordwise wing section containing the point $(x, y) = (0{\cdot}5648, -0{\cdot}0977)$ the slope of the oscillatory mode is given by

$$\frac{d}{dx}(lf_v) = -1 \qquad 6{\cdot}29$$

on the wing.

The nodal line for the in-wind vibration mode for the NLR wing with underwing store is presented in Figure 19. Comparison of Figure 9a with Figure 19 shows that the nodal line of Figure 19 is very similar to that of the clean wing at Mach number $M = 0{\cdot}6$ and frequency $F = 20$ Hz. Note that the vertical displacement of the store was taken equal to the displacement of the wing at location $(x, y) = (0{\cdot}430, 0{\cdot}477)$.

The unsteady spanwise normal force distribution on the wing in the presence of the underwing store has been calculated by the present method. The equation for the normal force distribution has been defined in Equation 6·17. Figure 20 shows the unsteady local normal force distribution calculated by the present method and compares it with the results of NLR doublet lattice calculations and experimental data [Ref. 13, Part IV]. As for the two previous cases involving the NLR wing combination (described in Sections 6·3 and 6·4), excellent agreement has been obtained between the present method and the NLR doublet lattice method for calculations of the spanwise normal load distribution on the wing with underwing store. Even at the discontinuity caused by the presence of the pylon, and where the nonplanar effects are the greatest, the agreement is very good. Once again, the experimental results yield a force distribution whose magnitude is less than that predicted by the theoretical methods.

When compared with the loading distribution on the clean wing, the nonplanar interference due to the pylon and store placed beneath the wing has a pronounced effect. The aerodynamic interference is responsible for an increase of the loading inboard of the pylon and a decrease on the outboard side. A discontinuity or jump in the real part of the normal load distribution also occurs at the pylon station. However, no such discontinuity is present in the imaginary part.

The forces and moments acting on the store and pylon assembly have been calculated using the present method, and are defined by the following equations

$$Z = \frac{\pi}{2}\rho V^2 \bar{c} s\, C_Z\, \theta\, e^{i\omega t} \qquad 6{\cdot}30$$

$$M = \frac{\pi}{4}\rho V^2 \bar{c}^2 s\, C_M\, \theta\, e^{i\omega t} \qquad 6{\cdot}31$$

$$Y = \frac{\pi}{2}\rho V^2 \bar{c} s\, C_Y\, \theta\, e^{i\omega t} \qquad 6{\cdot}32$$

$$N = \frac{\pi}{4}\rho V^2 \bar{c}^2 s\, C_N\, \theta\, e^{i\omega t} \qquad 6{\cdot}33$$

where C_Z is the normal force coefficient (positive in the positive z-direction),

C_M is the pitching moment coefficient about the balance centre (positive nose up);

C_Y is the side force coefficient (positive in the positive y-direction);

C_N is the yawing moment coefficient about the balance centre (positive nose in the positive y-direction);

$\bar{c}$ is the mean geometric chord ($\bar{c} = 0{\cdot}4183$ m)

s is the semi-span ($s = 0{\cdot}6226$ m).

The force and moment coefficients are given by:

$$C_Z = \frac{2l^2}{\pi \bar{c} s} \sum_k \lambda_k \cos \gamma_k A_k \qquad 6\cdot34$$

$$C_M = -\frac{4l^3}{\pi \bar{c}^2 s} \sum_k \lambda_k \cos \gamma_k A_k (x_k - x_{BAL}) / \qquad 6\cdot35$$

$$C_Y = -\frac{2l^2}{\pi \bar{c} s} \sum_k \lambda_k \sin \gamma_k A_k \qquad 6\cdot36$$

$$C_N = \frac{4l^3}{\pi \bar{c}^2 s} \sum_k \lambda_k \sin \gamma_k A_k (x_k - x_{BAL}) / \qquad 6\cdot37$$

where x_{BAL} is the dimensional x-ordinate of the balance centre ($x_{BAL} = 0{\cdot}430$ m). The variables λ_k, γ_k, A_k and x_k are as defined in Section 6·4 (Equations 6·25 and 6·26), and the summation is taken over all panels on the store, launcher and pylon assembly.

Table 7 presents the unsteady force and moment coefficients obtained by the present method and compares them with theoretical and experimental results obtained by Tijdeman *et al.* [Ref. 13, Part IV]. When compared with the NLR doublet lattice method, the present method yields coefficients which are from $1{\cdot}6\%$ to $46{\cdot}1\%$ greater in magnitude. In contrast to this, the phase angles exhibit considerably better agreement, the differences being less than $2{\cdot}05^\circ$. This behaviour is similar to that described for the tipstore in Section 6·4.

For a further discussion of the differences between theoretical calculations with the present method and the NLR doublet lattice method, the reader is referred to Section 7.

6.6 Aligned Panels for NLR Wing with Store Configurations

In the application of the doublet lattice method to lifting surface combinations that are coplanar it is essential that the panels be aligned in streamwise strips. For nonplanar configurations this requirement may be relaxed as long as the wakes of panels do not cross and cause a singularity that is not located at the centre of the integration interval of the panels. It must, however, be noted that for nonplanar panel combinations which are in close proximity to each other, such a configuration will lead to a more complex variation of the planar and nonplanar parts of the Kernel function.

From an inspection of Figure 15 it is apparent that the streamwise edges of panels on the canard fins and aft wings of the tipstore do not line up in streamwise strips with the panels that comprise the launcher and missile body. A similar situation exists in Figure 18, where the panels on the canard fins and aft wings of the underwing store do not line up in streamwise strips with the nearby panels on the launcher, the store body and the wing.

Two new panel distributions were created for the tipstore and pylon store configurations, and they specifically embodied the feature that all planar and nonplanar panels were aligned in streamwise strips. The aligned panel distribution for the wing with tipstore is illustrated in Figure 21, and was created simply by modifying the spanwise distribution of panels on the launcher and missile body, increasing the total number of panels from 255 to 306. Figure 22 shows the aligned panel distribution for the wing with underwing store. This new panel distribution increased the number of panels from 244 to 414, and most of the refinement in the panel distribution occurred on the launcher, missile body and the wing in the vicinity of the wing-pylon junction.

Table 8 presents the unsteady normal force and pitching moment coefficients obtained for the aligned panel distribution on the NLR wing with tipstore using the present method. The results are compared with those of the NLR doublet lattice method [13] and earlier calculations

using the present method, both of which did not have an aligned panel distribution. The coefficients have been calculated for a Mach number $M = 0{\cdot}6$ and frequency of oscillation $F = 20$ Hz. When comparing the two results obtained by the present method, it is evident that the normal force coefficients are in excellent agreement. The greatest relative difference occurs between the magnitudes of the pitching moment coefficients. Since the normal force coefficient was less sensitive to the change to an aligned panel distribution, the change in pitching moment reflects a change in the predicted centre of pressure. Note that it is common to see a greater change in a moment coefficient than the corresponding force coefficient when a relatively coarse panel distribution is refined.

An inspection of Figure 21 shows that the panel distribution on the surface representing the launcher and missile body has been considerably refined. In comparison to the non-aligned panel distribution shown in Figure 15, the number of panels on the launcher and missile body has been increased by a factor of 2·5. Since this aerodynamic surface is large in relation to the complete tipstore, and its panels make a large contribution to the pitching moment, it is reasonable to see a large variation in the pitching moment coefficient.

As the aligned panel distribution resulted in a considerably more refined panel distribution for the tipstore assembly, it is not possible to separate the effect of aligning the panels in streamwise strips from the overall effect of having a more refined panel distribution. As the results obtained using the aligned panel distribution are similar to those that would have been obtained with only a refinement in the panel distribution, there is no evidence of any numerical difficulties associated with the non-aligned panel distribution.

Table 9 presents the unsteady normal force, pitching moment, side force and yawing moment coefficients obtained for the NLR wing with underwing store using the present method and an aligned panel distribution. The results are compared with those of the NLR doublet lattice method [13] and earlier calculations using the present method, both of which did not have an aligned panel distribution. The coefficients have been calculated for a Mach number $M = 0{\cdot}6$ and frequency of oscillation $F = 20$ Hz.

As for the aligned panel distribution for the tipstore, the aligned panel distribution for the underwing store yields forces and moments that are in excellent agreement with those obtained for the non-aligned case. The largest relative differences occur in the results for the yawing moment coefficient, and all the phase angles experience only minor variation.

As mentioned previously for the NLR tipstore, the aligned panel distribution is much more refined than the original non-aligned distribution (see Fig. 21). In particular, the number of panels on the launcher has increased by a factor of three. Since this aerodynamic surface has a large surface area, it is not surprising to see that the predicted yawing moment coefficients have varied from those obtained for the non-aligned panel distribution. The relatively much smaller variation in the pitching moment coefficient is due to the reduced level of refinement of the panels on the underwing store that contribute to the pitching moment coefficient. As for the tipstore case, there is no evidence of any numerical instability in the calculations performed with the non-aligned panel distribution.

7. DISCUSSION

The present computational formulation of the doublet lattice method has been applied to many different lifting surface configurations. The various combinations analysed comprised a wing and tailplane in tandem, a *T*-tail, a wing in isolation, a wing with a tipstore and a wing with an underwing store. Of these many configurations the latter two represent the most complex nonplanar aerodynamic interaction analysed here, and they form particularly difficult test cases used in the evaluation of the present method.

The wide range of configurations that was analysed shows that the computer program DOUBLAT can handle most configurations, provided that they are idealised within the limitations imposed by the doublet lattice method. Although not considered in this report, full- or partial-span control surfaces may be included. Also, problems involving *H*-tails or twin fins may be analysed without additional difficulty.

When compared with [1], the present method has resulted in a significant improvement in the speed of computation of the matrix of aerodynamic influence coefficients. For the NLR wing with underwing store configuration (described in Section 6·5), the present method reduced the time spent in this phase of the computations by 39%. This improvement in computational speed has been achieved without any reduction in numerical accuracy.

The results obtained by the present method for planar, nonplanar and intersecting lifting surface combinations have been compared with the results of other workers in the field. The comparisons show that the results of the present method generally lie within the range of results obtained by the other methods. Problems with a small (non-zero) vertical separation between streamwise columns of panels [3] can be handled up to the point where the separation is negligibly small.

However, for the configurations involving a wing and tipstore (Section 6·4) and a wing and underwing store (Section 6·5), the comparisons indicate that a number of differences exist between the theoretical results of the present method and those of the NLR doublet lattice method. When compared with the results of the NLR calculations, the present method consistently predicts forces on the tipstore and underwing store that are larger in magnitude. There does not, however, appear to be any constant factor involved. Although the magnitudes are significantly different, the agreement in the predicted phase angles is excellent for all the forces and moments.

The possibility that the non-aligned nature of the panel distributions on the NLR tipstore and underwing store configurations was contributing to the differences in force and moment coefficients was investigated. Aligned panel distributions for both the tipstore and underwing store cases were created (Section 6·6), and the results of the calculations were compared with those obtained using the original panel distributions. The differences between the two sets of results appeared to be due to the refinement of the panel distributions which had occurred for the cases with the aligned panels. There was no indication of any numerical instabilities.

Another interesting point arises when the theoretical results for the force and moment distributions over the NLR wing are compared with experimental results. It is evident from Figures 11, 12, 13, 14, 17 and 20 that there is a trend for the theoretical methods to predict force and moment distributions whose magnitudes are greater than the experimental results. This trend is generally followed by the theoretical results of the present method when predicting forces acting on the tipstore and underwing store. A similar trend in the NLR doublet lattice predictions is not evident in the results that have been presented.

8. CONCLUSION

The present formulation of the doublet lattice method has been applied to a large variety of lifting surface combinations. As programmed at ARL, the method is generally applicable to nonplanar and nonparallel combinations of interfering lifting surfaces. The results of the present method have been compared with those obtained by other workers, and the comparisons show generally good agreement. However, for the test cases involving NLR wings with either a tipstore or an underwing store, the agreement between the predicted magnitudes of the forces acting on the store assemblies was not as good, although the phase angles were in excellent agreement.

REFERENCES

1. Waldman, W. — A FORTRAN program for the determination of unsteady airforces on general combinations of interfering lifting surfaces oscillating in subsonic flow. Aeronautical Research Laboratories, Structures Report 412, January 1985.

2. Albano, E. Rodden, W. P. — A doublet lattice method for calculating lift distributions on oscillating surfaces in subsonic flows. A.I.A.A. Journal, Vol. 7, No. 2, Feb. 1969, pp. 279 285; also Errata A.I.A.A. Journal, Vol. 7, No. 11, Nov. 1969, p. 2192.

3. Rodden, W. P. Giesing, J. P. Kalman, T. P. — Refinement of the nonplanar aspects of the subsonic doublet lattice lifting surface method. J. Aircraft, Vol. 9, No. 1, Jan. 1972, pp. 69 73.

4. Giesing, J. P. Kalman, T. P. Rodden, W. P. — Subsonic unsteady aerodynamics for general configurations: Part 1, Direct application of the nonplanar doublet lattice method. AFFDL-TR 71 5, Feb. 1971, Air Force Wright Flight Dynamics Lab., Wright-Patterson Air Force Base, Ohio.

5. Farrell, P. A. — FORTRAN programs for the determination of generalised airforces on interfering lifting surfaces oscillating in subsonic flow. Aeronautical Research Laboratories, Report SM345, August 1973.

6. Mangler, K. W. — Improper integrals in theoretical aerodynamics. R.A.E. Aero. Report 2424, June 1951.

7. Farrell, P. A. — A program for the computation of preliminary aerodynamic data for interfering lifting surfaces in steady subsonic flow. Aeronautical Research Laboratories, Structures Note 430, September 1976.

8. Davies, D. E. — Calculations of generalised airforces on two parallel lifting surfaces oscillating harmonically in subsonic flow. Aeronautical Research Council, R & M No. 3749, September 1972.

9. Albano, E. Perkinson, F. Rodden, W. P. — Subsonic lifting-surface theory aerodynamics and flutter analysis of interfering wing horizontal tail configurations, Parts I and 2. Air Force Flight Dynamics Laboratory, AFFDL TR 70 59, Wright-Patterson Air Force Base, Ohio, May 1970.

10. Kalman, T. P. Rodden, W. P. Giesing, J. P. — Application of the doublet lattice method to nonplanar configurations in subsonic flow. J. Aircraft, Vol 8, No 6, June 1971, pp 406 413

11. Hedman, S. G. Vortex lattice method for calculation of quasi steady state loadings on thin elastic wings.
Report 105, October 1965, Aeronautical Research Institute of Sweden.

12. Stark, V. J. E. Aerodynamic forces on a combination of a wing and a fin oscillating in subsonic flow.
S.A.A.B. Tech. Note 54, Sweden, 1964.

13. Tijdeman, H.
van Nunen, J. W. G.
Kraan, A. N.
Persoon, A. J.
Poestkoke, R.
Roos, R.
Schippers, P.
Siebert, C. M. Transonic wind tunnel tests on an oscillating wing with external stores.
Part I. General description.
Part II. The clean wing.
Part III. The wing with tip store.
Part IV. The wing with underwing store.
National Aerospace Laboratory NLR, The Netherlands.
NLR TR 78106 U or
AFFDL TR 78 194, Parts I IV, 1978.

14. Dwight, H. B. Tables of integrals and other mathematical data.
4th Edition, 1966, The Macmillan Company.

15. Abramowitz, M.
Stegun, I. A. Handbook of mathematical functions with formulas, graphs and mathematical tables.
8th Edition, 1972, Dover Publications.

APPENDIX A

Integration procedure when $r^2 > 0$ over the integration interval

When $r^2 > 0$ the finite part integrals of Equations 4·12 and 4·13 no longer apply. Hence, the normalwash influence coefficient relating the normalwash on the r'th receiving panel to the uniform pressure acting over the s'th sending panel becomes

$$C_{rs} = D_{rs}^{(1)} + D_{rs}^{(2)} \qquad \text{A·1}$$

where

$$D_{rs}^{(1)} = \int_{l_s} \frac{G^{(1)}}{r^2}\, dl \qquad \text{A·2}$$

$$D_{rs}^{(2)} = \int_{l_s} \frac{G^{(2)}}{r^2}\, dl \qquad \text{A·3}$$

$$G^{(1)} = \frac{\cos\beta_2}{4\pi} e^{\frac{\mu x_2}{U}} K_1 I_1 \qquad \text{A·4}$$

$$G^{(2)} = \frac{\cos\beta_2}{4\pi} e^{\frac{\mu x_2}{U}} K_2 I_2^* \qquad \text{A·5}$$

By subdividing l_s into n smaller subintervals, we may write

$$D_{rs}^{(1)} = \sum_{m=1}^{n} \frac{B_m}{A_m} \int_{l_m} \frac{G^{(1)}}{r^2}\, dl \qquad \text{A·6}$$

$$D_{rs}^{(2)} = \sum_{m=1}^{n} \frac{B_m}{A_m} \int_{l_m} \frac{G^{(2)}}{r^2}\, dl \qquad \text{A·7}$$

where the line integrals are now carried over n straight line segments between points $A_m = (x_{Am}, y_{Am}, z_{Am})$ and $B_m = (x_{Bm}, y_{Bm}, z_{Bm})$. Points A_1 and B_n represent the two ends of the interval l_s. For convenience the m subscripts will be dispensed with to give

$$D_{rs}^{(1)} = \frac{B_1}{A_1} \int_{l_1} \frac{G^{(1)}}{r^2}\, dl + \frac{1}{B_1} \int_{l_2} \frac{G^{(1)}}{r^2}\, dl \qquad \text{A·8}$$

$$D_{rs}^{(2)} = \frac{B_1}{A_1} \int_{l_1} \frac{G^{(2)}}{r^2}\, dl + \frac{B}{A} \int_{l_2} \frac{G^{(2)}}{r^2}\, dl \qquad \text{A·9}$$

Let the line between points $A: (x_A, y_A, z_A)$ and $B: (x_B, y_B, z_B)$ be represented by the parametric relationship

$$\mathbf{r}_{AB}(p) = X_{AB}(p)\ \mathbf{i} + Y_{AB}(p)\ \mathbf{j} + Z_{AB}(p)\ \mathbf{k} \qquad -1 \leq p \leq 1 \qquad \text{A·10}$$

where

$$X_{AB}(p) = \bar{x} + \tilde{x}p \qquad \bar{x} = (x_A + x_B)/2 \qquad \tilde{x} = (x_B - x_A)/2 \qquad \text{A·11}$$

$$Y_{AB}(p) = \bar{y} + \tilde{y}p \qquad \bar{y} = (y_A + y_B)/2 \qquad \tilde{y} = (y_B - y_A)/2 \qquad \text{A·12}$$

$$Z_{AB}(p) = \bar{z} + \tilde{z}p \qquad \bar{z} = (z_A + z_B)/2 \qquad \tilde{z} = (z_B - z_A)/2 \qquad \text{A·13}$$

Hence Equations A·8 and A·9 may be written as

$$I^{(1)} = \int_{-1}^{+1} \frac{G^{(1)}(x_1(p), y_1(p), z_1(p))}{y_1(p)^2 + z_1(p)^2} \frac{dl}{dp}\, dp \qquad \text{A·14}$$

$$I^{(2)} = \int_{-1}^{+1} \frac{G^{(2)}(x_1(p), y_1(p), z_1(p))}{(y_1(p)^2 + z_1(p)^2)^2} \frac{dl}{dp}\, dp \qquad \text{A·15}$$

where

$$x_1(p) = x_r - X_{AB}(p) \qquad \text{A·16}$$

$$y_1(p) = y_r - Y_{AB}(p) \qquad \text{A·17}$$

$$z_1(p) = z_r - Z_{AB}(p) \qquad \text{A·18}$$

$$\frac{dl}{dp} = \left(\frac{d\mathbf{r}_{AB}}{dp} \cdot \frac{d\mathbf{r}_{AB}}{dp}\right)^{1/2} = (\tilde{x}^2 + \tilde{y}^2 + \tilde{z}^2)^{1/2} \qquad \text{A·19}$$

and (x_r, y_r, z_r) is the location of the control point on the r'th receiving panel for the combination being considered.

By substituting Equations A·16, A·17, and A·18 into Equations A·14 and A·15 we obtain

$$I^{(1)} = \frac{dl}{dp} \int_{-1}^{+1} \frac{G^{(1)}(p)}{D(p)}\, dp \qquad \text{A·20}$$

$$I^{(2)} = \frac{dl}{dp} \int_{-1}^{+1} \frac{G^{(2)}(p)}{D(p)^2}\, dp \qquad \text{A·21}$$

where

$$D(p) = ap^2 + bp + c \qquad \text{A·22}$$

$$a = \tilde{y}^2 + \tilde{z}^2 \qquad \text{A·23}$$

$$b = -2[\tilde{y}(y_r - \bar{y}) + \tilde{z}(z_r - \bar{z})] \qquad \text{A·24}$$

$$c = (y_r - \bar{y})^2 + (z_r - \bar{z})^2 \qquad \text{A·25}$$

Now, in order to evaluate the integrals in Equations A·20 and A·21, let us represent $G^{(1)}(p)$ and $G^{(2)}(p)$ by second-order Lagrangian interpolation polynomials

$$G^{(1)} = \sum_{i=1}^{3} (a_i p^2 + b_i p + c_i)\, G^{(1)}(p_i) \qquad \text{A·26}$$

$$G^{(n)} = \sum_{i=1}^{n} (a_i p^2 + b_i p + c_i) G^{(n)}(p_i) \qquad \text{A-27}$$

where the abscissae p_i are the zeroes of the Legendre polynomial. The coefficients a_i, b_i and c_i may by calculated from

$$a_1 p^2 + b_1 p + c_1 = (p - p_2)(p - p_3)/(p_1 - p_2)(p_1 - p_3) \qquad \text{A-28}$$

$$a_2 p^2 + b_2 p + c_2 = (p - p_1)(p - p_3)/(p_2 - p_1)(p_2 - p_3) \qquad \text{A-29}$$

$$a_3 p^2 + b_3 p + c_3 = (p - p_1)(p - p_2)/(p_3 - p_1)(p_3 - p_2) \qquad \text{A-30}$$

by equating like powers of p. Thus we obtain

$$a_1 = 1/(p_1 - p_2)(p_1 - p_3) \quad b_1 = -(p_2 + p_3)a_1 \quad c_1 = p_2 p_3 a_1 \qquad \text{A-31}$$

$$a_2 = 1/(p_2 - p_1)(p_2 - p_3) \quad b_2 = -(p_1 + p_3)a_2 \quad c_2 = p_1 p_3 a_2 \qquad \text{A-32}$$

$$a_3 = 1/(p_3 - p_1)(p_3 - p_2) \quad b_3 = -(p_1 + p_2)a_3 \quad c_3 = p_1 p_2 a_3 \qquad \text{A-33}$$

where the abscissae p_i and coefficients a_i, b_i and c_i are presented in Table 10. By choosing the abscissae p_i to correspond to the abscissae in the common Gaussian quadrature formula

$$\int_{-1}^{+1} f(p)\,dp = \sum_{i=1}^{n} w_i f(p_i) \qquad \text{A-34}$$

it is anticipated that the integration accuracy will be maximised compared to any other choice of p_i.

By substituting Equations A-26 and A-27 into Equations A-20 and A-21 we obtain

$$I = \sum_{i=1}^{n} B^{(n)}(r_1, r_2, p_i) \qquad \text{A-35}$$

$$J = \sum_{i=1}^{n} D^{(n)}(r_1, r_2, p_i) \qquad \text{A-36}$$

where $A = \int_{-1}^{+1} \frac{1}{f^2}\,dp = a\int_{-1}^{+1} \frac{p^2}{f^2}\,dp + b\int_{-1}^{+1} \frac{p}{f^2}\,dp + c\int_{-1}^{+1} \frac{1}{f^2}\,dp$ A-37

$$B = a\int_{-1}^{+1} \frac{p^2}{f^2}\,dp + b\int_{-1}^{+1} \frac{p}{f^2}\,dp + c\int_{-1}^{+1} \frac{1}{f^2}\,dp \qquad \text{A-38}$$

$f^2 = Ap^2 + Bp + C$ in Equation A-22. From the tables of integrals presented by Dwight [14], we obtain the indefinite integral corresponding to the definite integrals in Equation A-37

$$\int \frac{dp}{f^2} = \frac{2}{(4AC - B^2)^{1/2}} \tan^{-1}\frac{B + 2Ap}{(4AC - B^2)^{1/2}} \qquad B^2 - 4AC < 0 \qquad \text{A-39}$$

$$\int \frac{dp}{f^2} = \frac{1}{(B^2 - 4AC)^{1/2}} \ln\frac{B + 2Ap - (B^2 - 4AC)^{1/2}}{B + 2Ap + (B^2 - 4AC)^{1/2}} \qquad B^2 - 4AC > 0 \qquad \text{A-40}$$

$$= \frac{-2}{b + 2ap}, \qquad b^2 - 4ac = 0 \qquad \text{A·41}$$

$$\int \frac{p}{D}\,dp = \frac{1}{2a}\ln|D| - \frac{b}{2a}\int \frac{1}{D}\,dp \qquad \text{A·42}$$

$$\int \frac{p^2}{D}\,dp = \frac{p}{a} - \frac{b}{2a^2}\ln D + \frac{b^2 - 2ac}{2a^2}\int \frac{1}{D}\,dp \qquad \text{A·43}$$

The indefinite integrals corresponding to the definite integrals in Equation A·38 are:

$$\int \frac{1}{D^2}\,dp = \frac{b + 2ap}{(4ac - b^2)D} + \frac{2a}{(4ac - b^2)}\int \frac{1}{D}\,dp, \qquad b^2 - 4ac \neq 0 \qquad \text{A·44}$$

$$\int \frac{p}{D^2}\,dp = -\frac{bp + 2c}{(4ac - b^2)D} - \frac{b}{(4ac - b^2)}\int \frac{1}{D}\,dp, \qquad b^2 - 4ac \neq 0 \qquad \text{A·45}$$

$$\int \frac{p^2}{D^2}\,dp = \frac{(b^2 - 2ac)p + bc}{a(4ac - b^2)D} + \frac{2c}{(4ac - b^2)}\int \frac{1}{D}\,dp, \qquad b^2 - 4ac \neq 0 \qquad \text{A·46}$$

$$\int \frac{1}{D^2}\,dp = -\frac{8a^3}{3(b + 2ap)^3}, \qquad b^2 - 4ac = 0 \qquad \text{A·47}$$

$$\int \frac{p}{D^2}\,dp = -\frac{2a^2}{(b + 2ap)^2} - \frac{b}{2a}\int \frac{1}{D^2}\,dp, \qquad b^2 - 4ac = 0 \qquad \text{A·48}$$

$$\int \frac{p^2}{D^2}\,dp = -\frac{4a^2p}{(b + 2ap)^2} - \frac{b^2}{4a^2}\int \frac{1}{D^2}\,dp, \qquad b^2 - 4ac = 0 \qquad \text{A·49}$$

Note that since D^2 represents the variation of $r^2 = y_1^2 + z_1^2$ over the interval l, then $D^2 > 0$. Thus the determinant $b^2 - 4ac$ is less than or equal to zero for all practical cases of interest and, therefore, we may neglect any integrals obtained for the case $b^2 - 4ac > 0$.

APPENDIX B

Integration procedure when $r^2 = 0$ in the centre of the integration interval

In the doublet lattice method, when the $r^2 = 0$ singularity occurs it must do so in the centre of the interval l_s over which the integration of Equation 2·4 is defined. Following the method of Appendix A, the interval l_s may be subdivided into n smaller intervals. Furthermore, if we assume that the singularity falls symmetrically within the i'th interval, then the downwash influence coefficient may be written as

$$D_{rs} = D_{rs}^{(1)} + D_{rs}^{(2)} \qquad \text{B·1}$$

where

$$D_{rs}^{(1)} = \sum_{m=1}^{i-1} \int_{A_m}^{B_m} \frac{G^{(1)}}{r^2}\,dl + \int_{A_i}^{B_i} \frac{G^{(1)}}{r^2}\,dl + \sum_{m=i+1}^{n} \int_{A_m}^{B_m} \frac{G^{(1)}}{r^2}\,dl \qquad \text{B·2}$$

$$D_{rs}^{(2)} = \sum_{m=1}^{i-1} \int_{A_m}^{B_m} \frac{G^{(2)}}{r^2}\,dl + \int_{A_i}^{B_i} \frac{G^{(2)}}{r^4}\,dl + \sum_{m=i+1}^{n} \int_{A_m}^{B_m} \frac{G^{(2)}}{r^4}\,dl \qquad \text{B·3}$$

The line integrals are evaluated over n straight line segments between points $A_m: (x_{Am}, y_{Am}, z_{Am})$ and $B_m: (x_{Bm}, y_{Bm}, z_{Bm})$. Points A_1 and B_n represent the two end points of the interval l_s.

The integrals in the first and third terms of Equations B·2 and B·3 may be evaluated using the method described in Appendix A. It now remains to derive a method for solving the finite part integrals in Equations B·2 and B·3. If we dispense with the subscript i then the integrals of interest are

$$I^{(1)} = \int_{A_i}^{B_i} \frac{G^{(1)}}{r^2}\,dl \qquad \text{B·4}$$

$$I^{(2)} = \int_{A_i}^{B_i} \frac{G^{(2)}}{r^2}\,dl \qquad \text{B·5}$$

Now since $r^2 = 0$ in the centre of the interval from point $A: (x_A, y_A, z_A)$ to point $B: (x_B, y_B, z_B)$, the line between these two points can be expressed by the parametric relationship

$$\mathbf{r}_{AB}(p) = X_{AB}(p)\,\mathbf{i} + Y_{AB}(p)\,\mathbf{j} + Z_{AB}(p)\,\mathbf{k} \qquad -1 \le p \le 1 \qquad \text{B·6}$$

where

$$X_{AB}(p) = \bar{x} + \hat{x}p \qquad \hat{x} = (x_B - x_A)/2 \qquad \bar{x} = (x_A + x_B)/2 \qquad \text{B·7}$$

$$Y_{AB}(p) = \bar{y} + \hat{y}p \qquad \hat{y} = (y_B - y_A)/2 \qquad \bar{y} = y_i \qquad \text{B·8}$$

$$Z_{AB}(p) = \bar{z} + \hat{z}p \qquad \hat{z} = (z_B - z_A)/2 \qquad \bar{z} = z_i \qquad \text{B·9}$$

and the control point for the panel combination is located at (x_r, y_r, z_r). Note that when $r^2 = 0$ the control point on the receiving panel and the lift point on the sending panel (shown in Fig. 4) lie on the same streamwise line.

Using the above definitions of $X_{AB}(p)$, $Y_{AB}(p)$ and $Z_{AB}(p)$ we obtain

$$x_1(p) = x_r - (\bar{x} + \tilde{x}p) \qquad \text{B·10}$$

$$y_1(p) = -\tilde{y}p \qquad \text{B·11}$$

$$z_1(p) = -\tilde{z}p \qquad \text{B·12}$$

Hence we see that $r^2 = y_1^2 + z_1^2$ is simply

$$r^2 = (\tilde{y}^2 + \tilde{z}^2)p^2 \qquad \text{B·13}$$

and, as in Appendix A, we have that

$$\frac{dl}{dp} = (\tilde{x}^2 + \tilde{y}^2 + \tilde{z}^2)^{1/2} \qquad \text{B·14}$$

Thus Equations B·4 and B·5 become

$$I^{(1)} = \frac{1}{\tilde{y}^2 + \tilde{z}^2}\frac{dl}{dp}\int_{-1}^{+1} \frac{G^{(1)}(p)}{p^2}\,dp \qquad \text{B·15}$$

$$I^{(2)} = \frac{1}{\tilde{y}^2 + \tilde{z}^2}\frac{dl}{dp}\int_{-1}^{+1} \frac{G^{(2)}(p)}{p^4}\,dp \qquad \text{B·16}$$

Following the method of Farrell [5], the numerators $G^{(1)}(p)$ and $G^{(2)}(p)$ may be approximated by polynomials of order $(n-1)$

$$G^{(1)}(p) = \sum_{i=1}^{n}\sum_{j=1}^{n} h_{ji}\,p^{j-1}\,G^{(1)}(p_i) \qquad \text{B·17}$$

$$G^{(2)}(p) = \sum_{i=1}^{n}\sum_{j=1}^{n} h_{ji}\,p^{j-1}\,G^{(2)}(p_i) \qquad \text{B·18}$$

where the h_{ji} are the coefficients of the polynomial. The abscissae p_i are the roots of the n'th order Tchebycheff polynomial of the first kind. The abscissae may be determined from the following equation [Ref. 15, p. 889]

$$p_i = -\cos\frac{(2i-1)\pi}{2n} \qquad \text{B·19}$$

By substituting Equations B·17 and B·18 into Equations B·15 and B·16 we obtain

$$I^{(1)} = \frac{1}{\tilde{y}^2 + \tilde{z}^2}\frac{dl}{dp}\sum_{i=1}^{n} C_i^{(1)}\,G^{(1)}(p_i) \qquad \text{B·20}$$

$$I^{(2)} = \frac{1}{\tilde{y}^2 + \tilde{z}^2}\frac{dl}{dp}\sum_{i=1}^{n} C_i^{(2)}\,G^{(2)}(p_i) \qquad \text{B·21}$$

where

$$C_i^{(1)} = \sum_{j=1}^{n} h_{ji} \int_{-1}^{+1} p^{j-1}\, dp \qquad \text{B-22}$$

$$C_i^{(2)} = \sum_{j=1}^{n} h_{ji} \int_{-1}^{+1} p^{j-1}\, dp \qquad \text{B-23}$$

By equating like powers of p, the h_{ji} may be calculated from

$$\sum_{j=1}^{n} h_{ji}\, p^{j-1} = \frac{\prod_{\substack{u=1 \\ u \neq i}}^{n} (p - p_u)}{\prod_{\substack{v=1 \\ v \neq i}}^{n} (p_i - p_v)}, \quad i = 1, 2, \ldots, n \qquad \text{B-24}$$

As in Reference 5, an eighth order polynomial has been chosen. This corresponds to $n = 9$, and the abscissae p_i and the weights $C_i^{(1)}$ and $C_i^{(2)}$ have been calculated and are listed in Table 11.

TABLE 1

Values of Generalised Airforces, Q_{pq}, for the AGARD Wing-Tailplane Configuration (for $h = 0$) as Obtained by Different Workers

$h = 0$ $M = 0{\cdot}8$	Q_{pq}	Davies	Albano Perkinson Rodden	Albano Rodden	Giesing Kalman Rodden	Farrell	Present Method (1)	Present Method (2)
$k = 0$	$\lvert Q_{11}\rvert$	0·4403	0·4425	0·4554	0·4401	0·4377	0·4551	0·4557
	$\angle Q_{11}$	359·9	359·9	359·9	359·9	360·0	360·0	360·0
	$\lvert Q_{12}\rvert$	0·6202	0·6121	0·6655	0·6557	0·6457	0·6654	0·6653
	$\angle Q_{12}$	180·0	180·0	180·0	180·0	180·0	180·0	180·0
	$\lvert Q_{21}\rvert$	0·1046	0·1054	0·1107	0·1044	0·1049	0·1109	0·1083
	$\angle Q_{21}$	180·3	180·3	180·3	180·3	180·0	180·0	180·0
	$\lvert Q_{22}\rvert$	0·1759	0·1954	0·2237	0·2126	0·2184	0·2235	0·2261
	$\angle Q_{22}$	180·2	180·2	180·2	180·2	180·0	180·0	180·0
$k = 1{\cdot}5$	$\lvert Q_{11}\rvert$	1·5865	1·6022	1·5496	1·5688	1·4212	1·5187	1·5714
	$\angle Q_{11}$	314·2	314·4	311·2	310·7	312·3	311·7	310·8
	$\lvert Q_{12}\rvert$	0·9180	0·8910	0·9081	0·9495	0·8752	0·9006	0·9484
	$\angle Q_{12}$	265·5	266·3	267·2	265·4	265·0	267·1	265·8
	$\lvert Q_{21}\rvert$	1·0043	1·0099	1·0550	1·0511	0·9507	1·0250	1·0654
	$\angle Q_{21}$	291·7	291·4	287·2	288·5	289·9	288·2	289·0
	$\lvert Q_{22}\rvert$	1·2845	1·2386	1·2144	1·2719	1·1448	1·1906	1·2747
	$\angle Q_{22}$	294·7	294·3	293·7	292·9	294·1	294·0	293·2

TABLE 2

Values of Generalised Airforces, Q_{pq}, for the AGARD Wing-Tailplane Configuration as Obtained by Different Workers

$h = 0{\cdot}6$ $M = 0{\cdot}8$	Q_{pq}	Davies	Albano Perkinson Rodden	Farrell	Present Method (1)	Present Method (2)
$k = 0$	Q_{11}	0·1470	0·1490	0·1374	0·1425	0·1432
	Q_{11}	359·8	359·8	360·0	360·0	360·0
	Q_{12}	0·6402	0·6312	0·6661	0·6866	0·6868
	Q_{12}	180·1	180·1	180·0	180·0	180·0
	Q_{21}	0·2404	0·2405	0·2527	0·2674	0·2669
	Q_{21}	180·1	180·1	180·0	180·0	180·0
	Q_{22}	0·1619	0·1817	0·1958	0·2093	0·2117
	Q_{22}	180·3	180·2	180·0	180·0	180·0
$k = 1{\cdot}5$	Q_{11}	1·1009	1·1200	0·9780	1·0475	1·0838
	Q_{11}	301·3	301·3	299·9	298·8	298·3
	Q_{12}	1·1342	1·1128	1·0735	1·1072	1·1584
	Q_{12}	251·7	251·9	249·5	250·6	250·0
	Q_{21}	0·9072	0·9122	0·8259	0·8937	0·9241
	Q_{21}	278·0	277·7	276·9	275·1	275·8
	Q_{22}	1·3867	1·3397	1·2082	1·2607	1·3543
	Q_{22}	289·2	288·6	287·2	286·9	286·4

TABLE 3

Generalised Airforces for the AGARD Wing-Tailplane Configuration for Various Values of Vertical Separation, h, Between Wing and Tailplane

$k=1\cdot5$ $M=0\cdot8$	$\lvert Q_{11}\rvert$ $\angle Q_{11}$		$\lvert Q_{12}\rvert$ $\angle Q_{12}$		$\lvert Q_{21}\rvert$ $\angle Q_{21}$		$\lvert Q_{22}\rvert$ $\angle Q_{22}$	
h	Davies	Present Method (2)	Davies	Present Method (2)	Davies	Present Method (2)	Davies	Present Method (2)
0	1·5865 314·2	1·5714 310·8	0·9180 265·5	0·9484 265·8	1·0043 291·7	1·0654 289·0	1·2845 294·7	1·2747 293·2
0·01	1·5519 313·3	1·5514 310·7	0·9332 264·0	0·9524 264·9	0·9973 290·4	1·0577 288·7	1·2890 294·0	1·2736 292·8
0·04	1·4773 311·4	1·4782 309·3	0·9640 261·2	0·9789 261·7	0·9843 287·7	1·0350 286·6	1·2992 292·6	1·2783 291·3
0·1	1·3730 308·7	1·3606 306·1	1·0040 258·0	1·0304 257·5	0·9662 284·3	1·0043 282·8	1·3151 291·3	1·2947 289·2
0·2	1·2624 305·9	1·2463 303·0	1·0479 255·2	1·0780 254·1	0·9428 281·4	0·9726 279·5	1·3376 290·4	1·3140 287·8
0·3	1·1948 304·0	1·1788 301·2	1·0790 253·7	1·1073 252·3	0·9271 279·8	0·9521 277·8	1·3559 290·0	1·3271 287·2
0·4	1·1511 302·8	1·1350 299·9	1·1024 252·8	1·1285 251·2	0·9174 279·0	0·9384 276·8	1·3695 289·7	1·3377 286·9
0·5	1·1216 301·9	1·1049 299·0	1·1204 252·2	1·1452 250·5	0·9113 278·4	0·9296 276·2	1·3795 289·5	1·3469 286·6
0·6	1·1009 301·3	1·0838 298·3	1·1342 251·7	1·1584 250·0	0·9072 278·0	0·9241 275·8	1·3867 289·2	1·3543 286·4

TABLE 4

Generalised Airforces for Stark's T-tail for Zero Frequency, and Two Mach Numbers as Obtained by Different Workers

	$k=0$ $M=0$			$k=0$ $M=0\cdot8$		
Q_{pq}	Stark	Kalman Rodden Giesing	Present Method	Stark	Kalman Rodden Giesing	Present Method
Q_{11}	−0·6220	−0·6095	−0·5436	−0·8137	−0·7804	−0·7203
Q_{21}	−3·2503	−3·3647	−3·4032	−3·7366	−3·8768	−3·8941
Q_{31}	−0·7813	−0·7965	−0·8230	−0·7858	−0·7985	−0·8257

TABLE 5

Generalised Airforces for Stark's *T*-tail as Obtained by Different Workers

	$k = 0{\cdot}6$ $M = 0{\cdot}8$						$k = 0{\cdot}9$ $M = 0{\cdot}8$		
Q_{pq}	Stark	Davies	Zwaan	Kalman Rodden Giesing	Farrell	Present Method	Stark	Farrell	Present Method
Q_{11}	3·0826	3·2421	3·2873	3·3527	2·7470	3·0975	4·8800	4·1775	4·8070
Q_{11}	258·8	260·6	259·8	261·0	260·6	260·4	264·9	266·2	265·5
Q_{12}	0·3202	0·3399	0·3475	0·3431	0·2799	0·3215	0·7020	0·6016	0·7045
Q_{12}	323·9	328·5	327·4	329·4	328·1	328·1	330·6	333·7	332·7
Q_{13}	0·1695	0·1859	0·1865	0·1830	0·1680	0·1828	0·3214	0·2971	0·3358
Q_{13}	62·4	61·5	60·8	61·9	61·6	60·9	52·0	50·4	49·7
Q_{21}	4·4628	4·5670	4·5650	4·6612	4·4291	4·6103	5·3736	5·1126	5·4491
Q_{21}	210·7	211·1	210·9	212·3	211·0	211·0	220·8	220·1	221·2
Q_{22}	0·7758	0·7930	0·7936	0·8134	0·7815	5708·0	1·2419	1·2185	1·2827
Q_{22}	281·2	282·1	281·9	283·3	282·3	282·2	286·5	288·3	287·6
Q_{23}	0·2103	0·2191	0·2183	0·2269	0·2282	0·2331	0·3692	0·3882	0·4055
Q_{23}	298·2	299·0	298·9	298·3	296·6	297·8	310·2	307·6	309·0
Q_{31}	1·0772	1·1154	1·1006	1·1383	1·1483	1·1686	1·3760	1·4446	1·4904
Q_{31}	222·7	224·7	224·6	224·9	225·3	224·9	232·1	236·6	235·3
Q_{32}	0·1810	0·1897	0·1874	0·1948	0·2000	0·2022	0·3214	0·3484	0·3557
Q_{32}	297·7	299·8	299·7	299·8	300·1	299·7	305·8	308·5	307·6
Q_{33}	0·3319	0·3349	0·3349	0·3523	0·3590	0·3618	0·5484	0·5794	0·5911
Q_{33}	289·8	289·6	289·6	289·4	288·8	289·4	298·1	296·8	297·5

TABLE 6

Comparison of Unsteady Loads on the NLR Wing with Tipstore for M = 0·6 and M = 0·8 at F = 20Hz

$M = 0{\cdot}6$ $k = 0{\cdot}4$ $F = 20$ Hz	NLR Experiment	NLR Doublet Lattice	Present Method
C_L	0·08374	0·08334	0·09286
C_I	11·71	5·51	6·05
C_M	0·04610	0·03298	0·04125
C_M	356·27	345·95	344·89

(*a*)

$M = 0{\cdot}8$ $k = 0{\cdot}3$ $F = 20$ Hz	NLR Experiment	NLR Doublet Lattice	Present Method
C_L	0·09831	0·09402	0·10733
C_I	9·37	1·22	1·65
C_M	0·04540	0·03324	0·04367
C_M	352·40	344·29	343·75

(*b*)

TABLE 7

Comparison of Unsteady Loads on the NLR Wing with Underwing Store for M 0·6 and F 20Hz

M 0·6 k 0·4 F 20 Hz	NLR Experiment	NLR Doublet Lattice	Present Method
C_L	0·01334	0·01118	0·01571
C_I	37·39	26·56	28·45
C_M	0·02223	0·02309	0·03374
C_M	341·65	342·35	342·10
C_Y	0·04612	0·05104	0·06146
C_Y	1·62	357·75	359·77
C_N	0·01900	0·00707	0·00718
C_N	179·52	171·87	169·86

TABLE 8

Comparison of Unsteady Loads on the NLR Wing with Tipstore Obtained Using Aligned and Non-aligned Panel Distributions

$M = 0{\cdot}6$ $k = 0{\cdot}4$ $F = 20$ Hz	NLR Doublet Lattice	Present Method	
		Non-aligned Panels	Aligned Panels
C_Z	0·08334	0·09286	0·09339
$\angle C_Z$	5·51	6·05	5·46
C_M	0·03298	0·04125	0·03571
$\angle C_M$	345·95	344·89	342·75

TABLE 9

Comparison of Unsteady Loads on the NLR Wing with Underwing Store Obtained Using Aligned and Non-aligned Panel Distributions

$M = 0{\cdot}6$ $k = 0{\cdot}4$ $F = 20$ Hz	NLR Doublet Lattice	Present Method	
		Non-aligned Panels	Aligned Panels
C_Y	0·01118	0·01571	0·01564
$\angle C_Y$	26·56	28·45	28·34
C_M	0·02309	0·03374	0·03354
$\angle C_M$	342·35	342·10	341·96
C_N	0·05104	0·06146	0·06261
$\angle C_N$	357·75	359·77	359·58
C_L	0·00707	0·00718	0·00647
$\angle C_L$	171·87	169·86	168·26

TABLE 10

Abscissae p_i and Coefficients a_i, b_i and c_i (for i = 1 to 3) Used in Integration Scheme When $r^2 > 0$

i	p_i	a_i	b_i	c_i
1	−0·774596669	0·833333333	−0·645497224	0·0
2	0·0	−1·666666667	0·0	1·0
3	+0·774596669	0·833333333	0·645497224	0·0

TABLE II

Abscissae p_i and Weights $C_i^{(1)}$ and $C_i^{(2)}$ for "Finite Part" Integration

$$\int_{-1}^{+1} \frac{f^{(1)}(p)}{p^2}\,dp \approx \sum_{i=1}^{9} C_i^{(1)} f^{(1)}(p_i)$$

$$\int_{-1}^{+1} \frac{f^{(2)}(p)}{p^4}\,dp \approx \sum_{i=1}^{9} C_i^{(2)} f^{(2)}(p_i)$$

i	p_i	$C_i^{(1)}$	$C_i^{(2)}$
1	−0·984807753	−0·007642844	2·523788807
2	−0·866025404	0·469841270	−8·800000000
3	−0·642787610	−0·003167376	26·207863447
4	−0·342020143	5·610810220	−65·620541147
5	0·0	−14·139682541	90·711111120
6	0·342020143	5·610810220	−65·620541147
7	0·642787610	−0·003167376	26·207863447
8	0·866025404	0·469841270	−8·800000000
9	0·984807753	−0·007642844	2·523788807

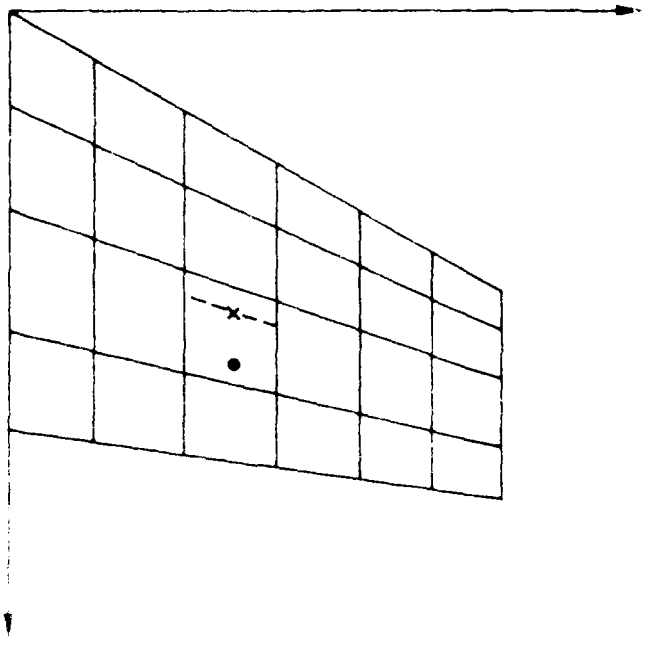

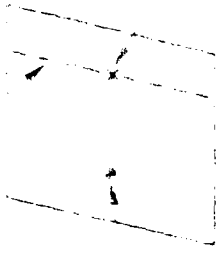

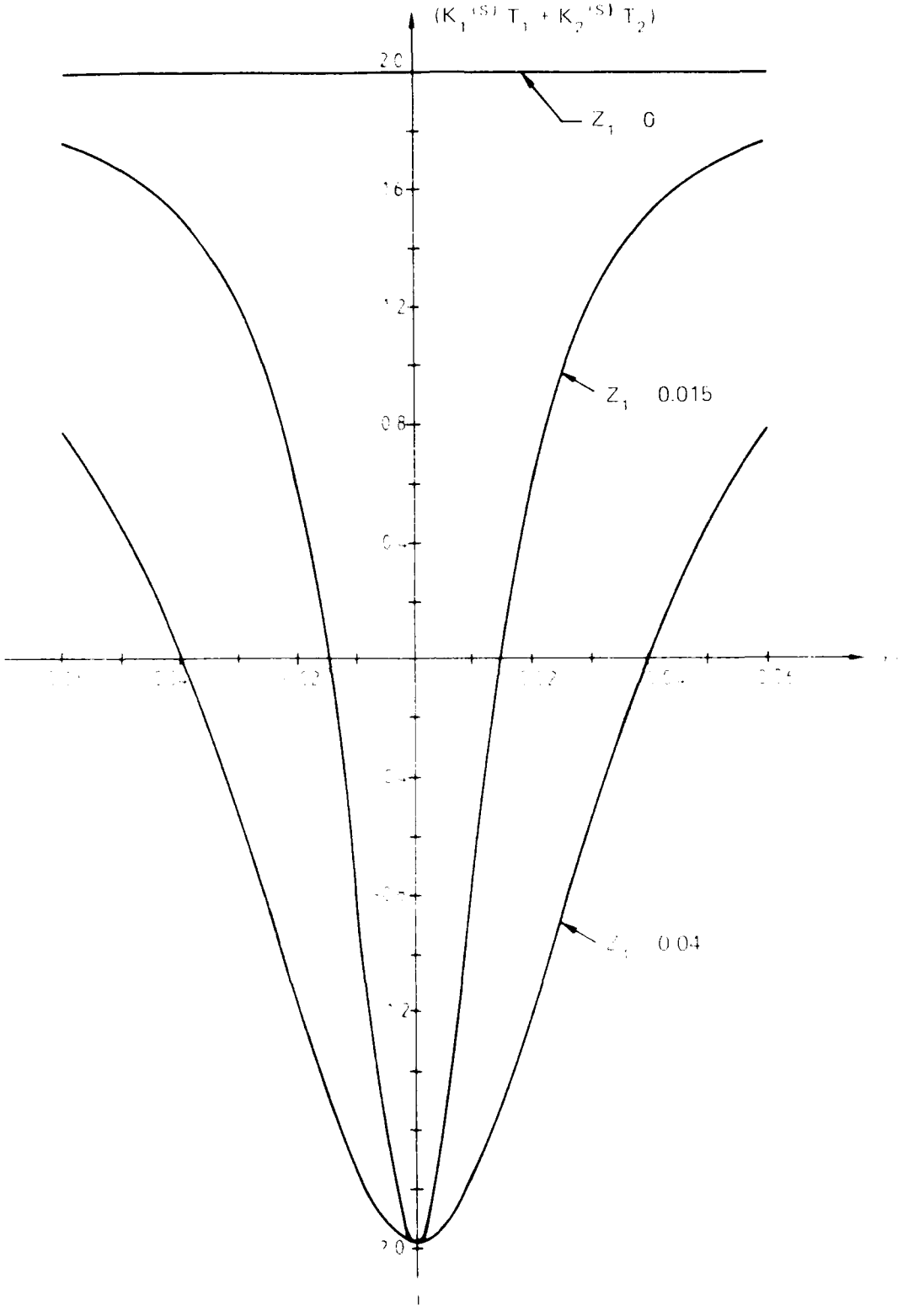

FIG. 2 PLOT OF THE NUMERATOR OF THE STEADY KERNEL FUNCTION, $(K_1^{(S)} T_1 + K_2^{(S)} T_2)$, AS A FUNCTION OF Y, FOR X, 0.5, M 0 AND THREE VALUES OF Z_1

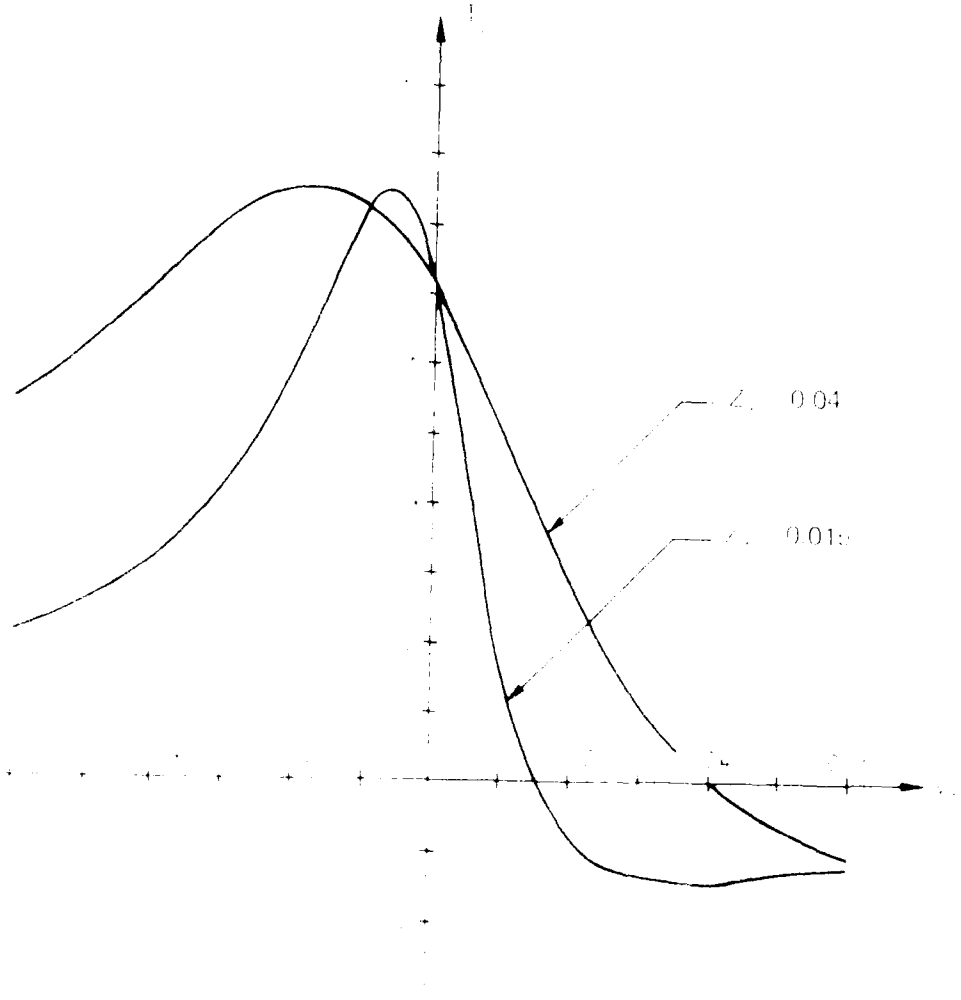
0.04

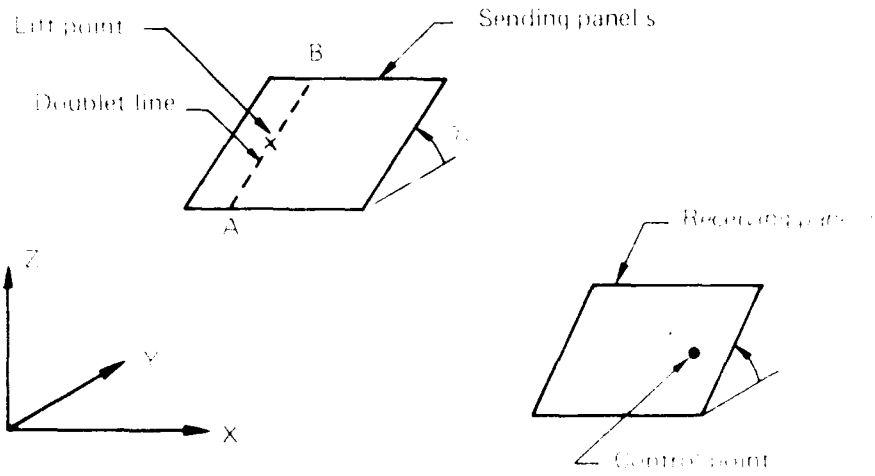

FIG. 4 DIAGRAM SHOWING A GENERAL COMBINATION OF A SENDING AND RECEIVING PANEL

Tail plane is h units above plane of wing
Reference length = semi span = 1.0

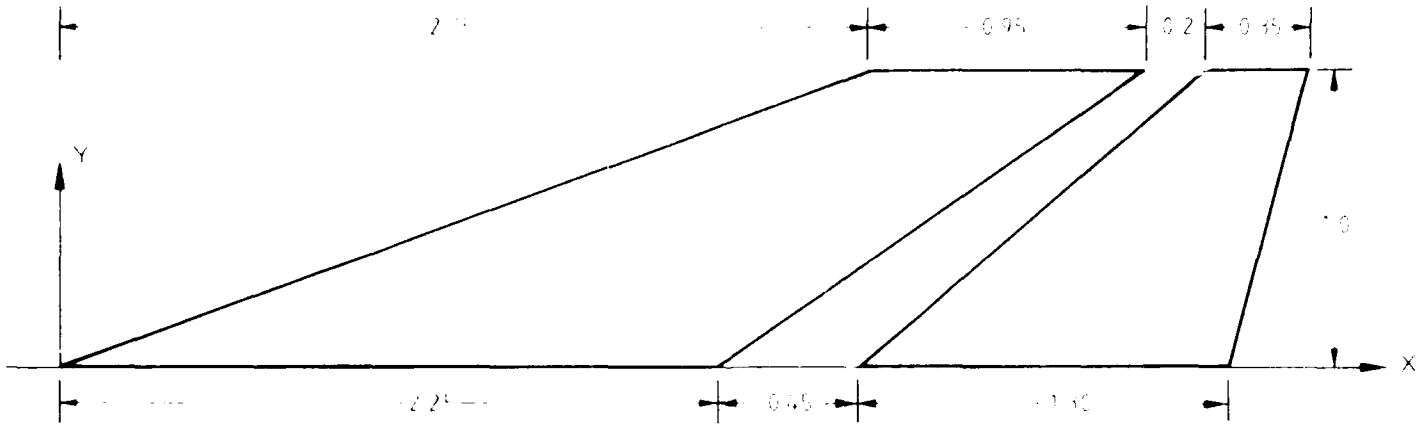

FIG. 5 AGARD HORIZONTAL WING TAILPLANE CONFIGURATION

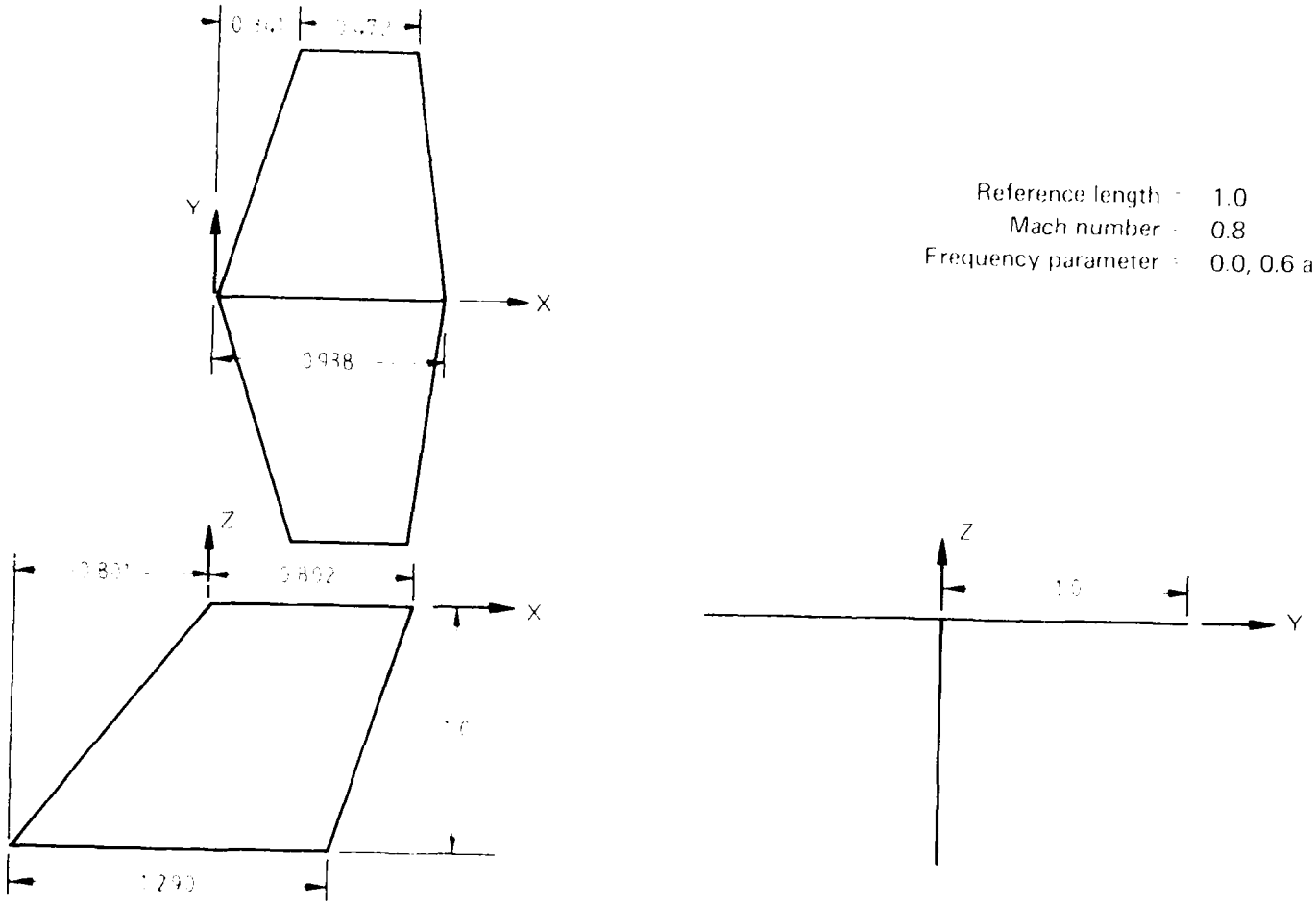

Reference length - 1.0
Mach number - 0.8
Frequency parameter - 0.0, 0.6 and 0.9

FIG. 6 STARK'S SWEPT AND TAPERED T TAIL CONFIGURATION.

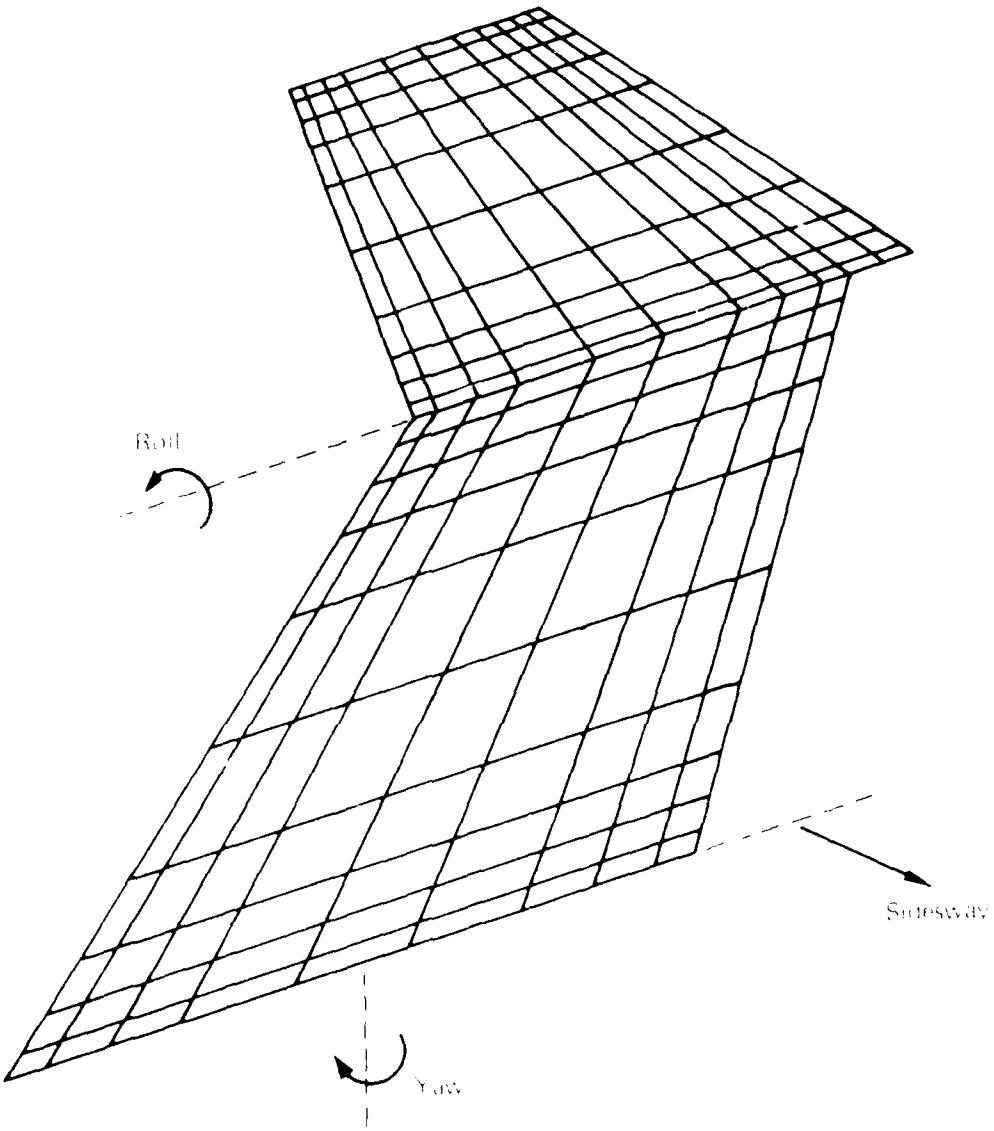

FIG. 7 PANEL DISTRIBUTION USED IN CALCULATING GENERALISED AIRFORCES FOR STARBOARD TAIL FORE CARRY ONLY THE STARBOARD HALF OF THE [illegible]

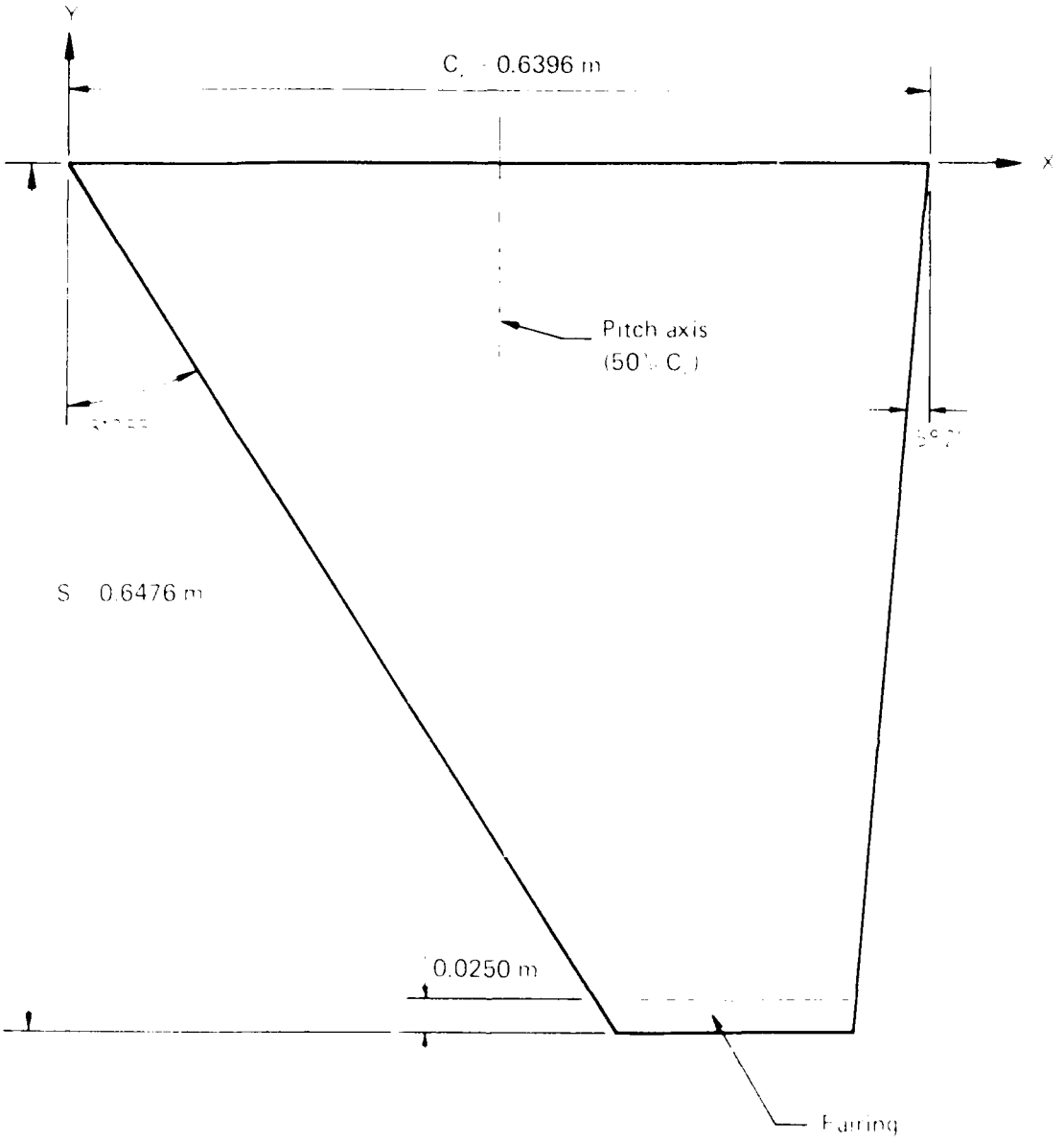

FIG. 3.8 SKETCH OF THE NLR CLEAN WING CONFIGURATION SHOWING THE PRINCIPAL DIMENSIONS.

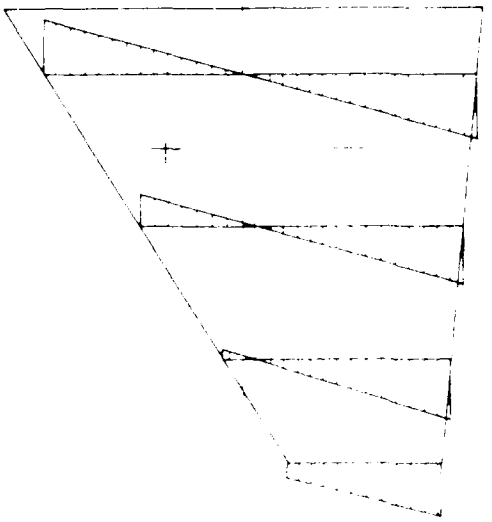

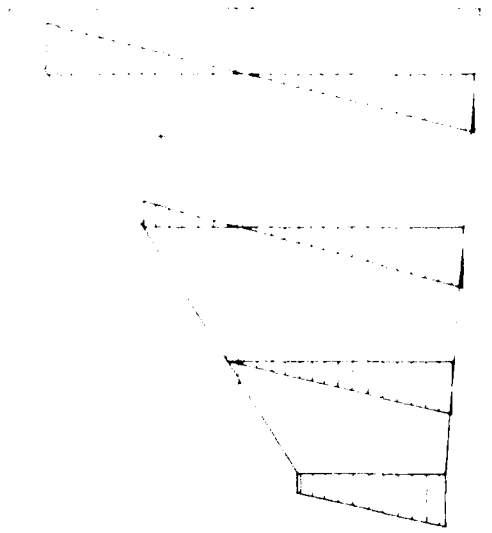

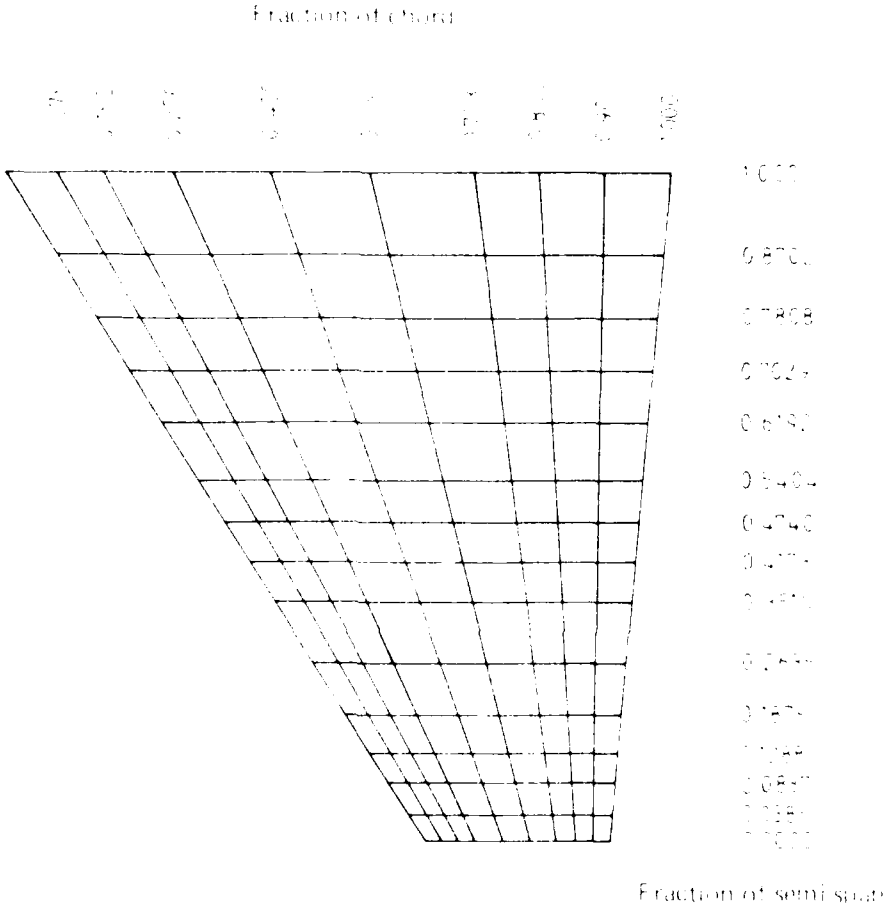

FIG. 10 PANEL DISTRIBUTION FOR THE NLR CLEAN WING USED IN THEORETICAL CALCULATIONS WITH THE DOUBLET LATTICE METHOD. CHORDWISE AND SPANWISE ORDINATES REPRESENT NONDIMENSIONAL FRACTIONS OF THE CHORD AND SPAN

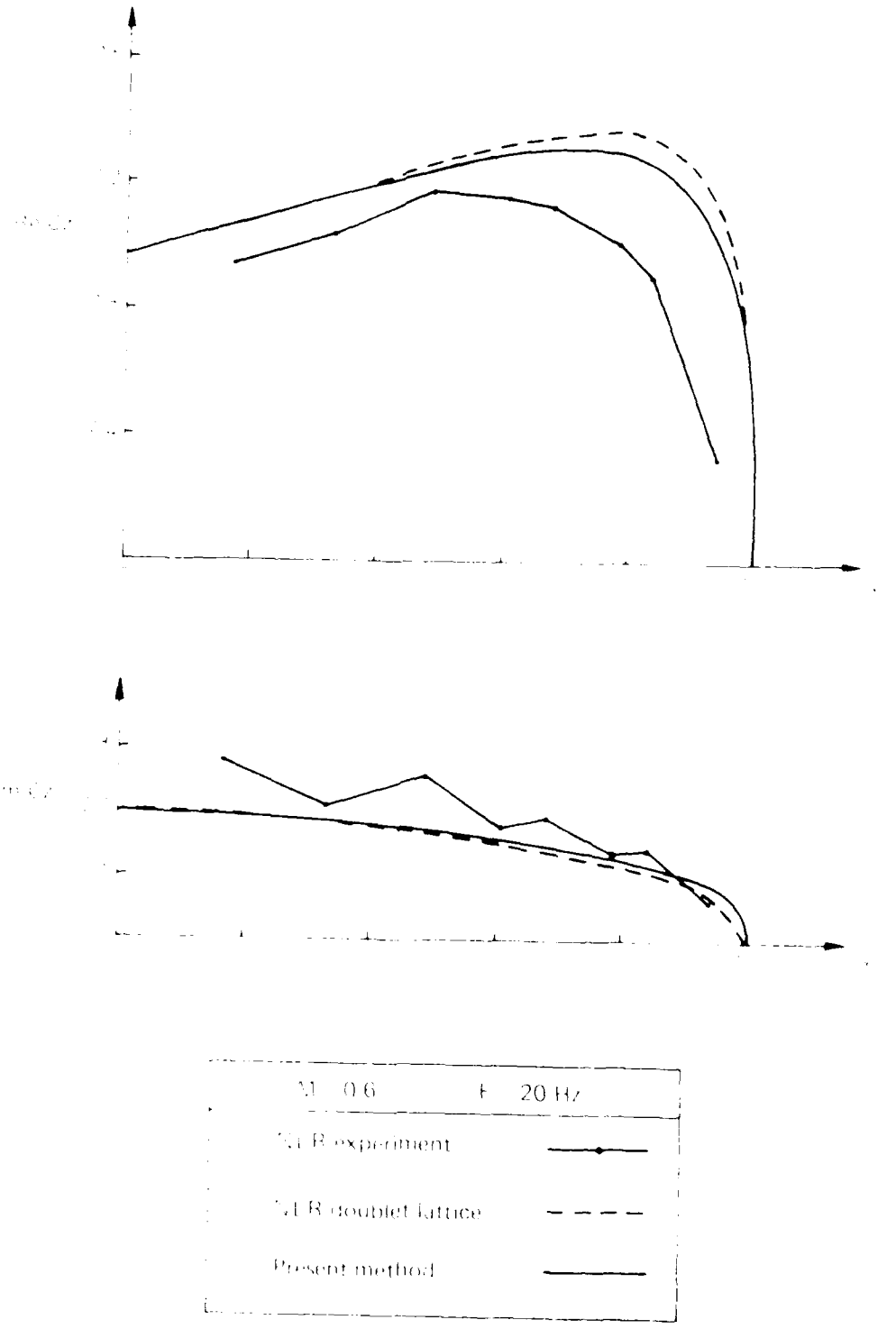

FIG. 11 UNSTEADY SPANWISE NORMAL FORCE DISTRIBUTION FOR THE CLEAN NLR WING AT M = 0.6 AND F = 20 Hz

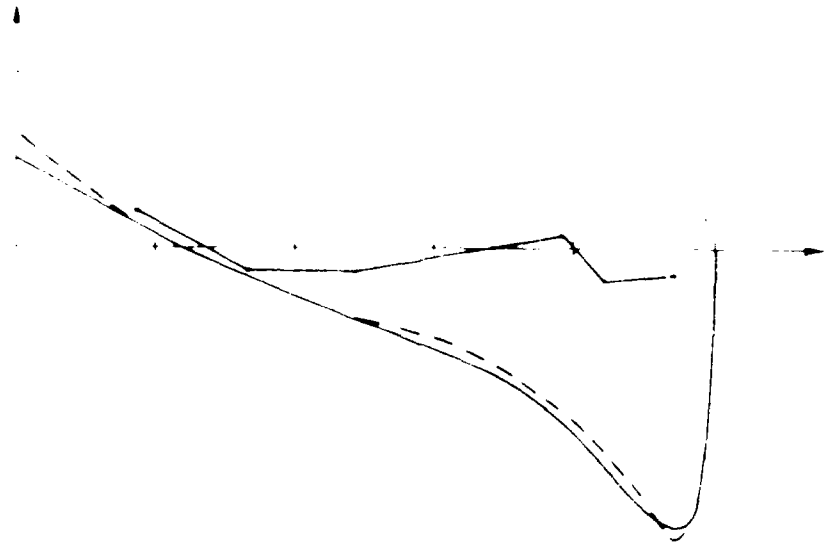

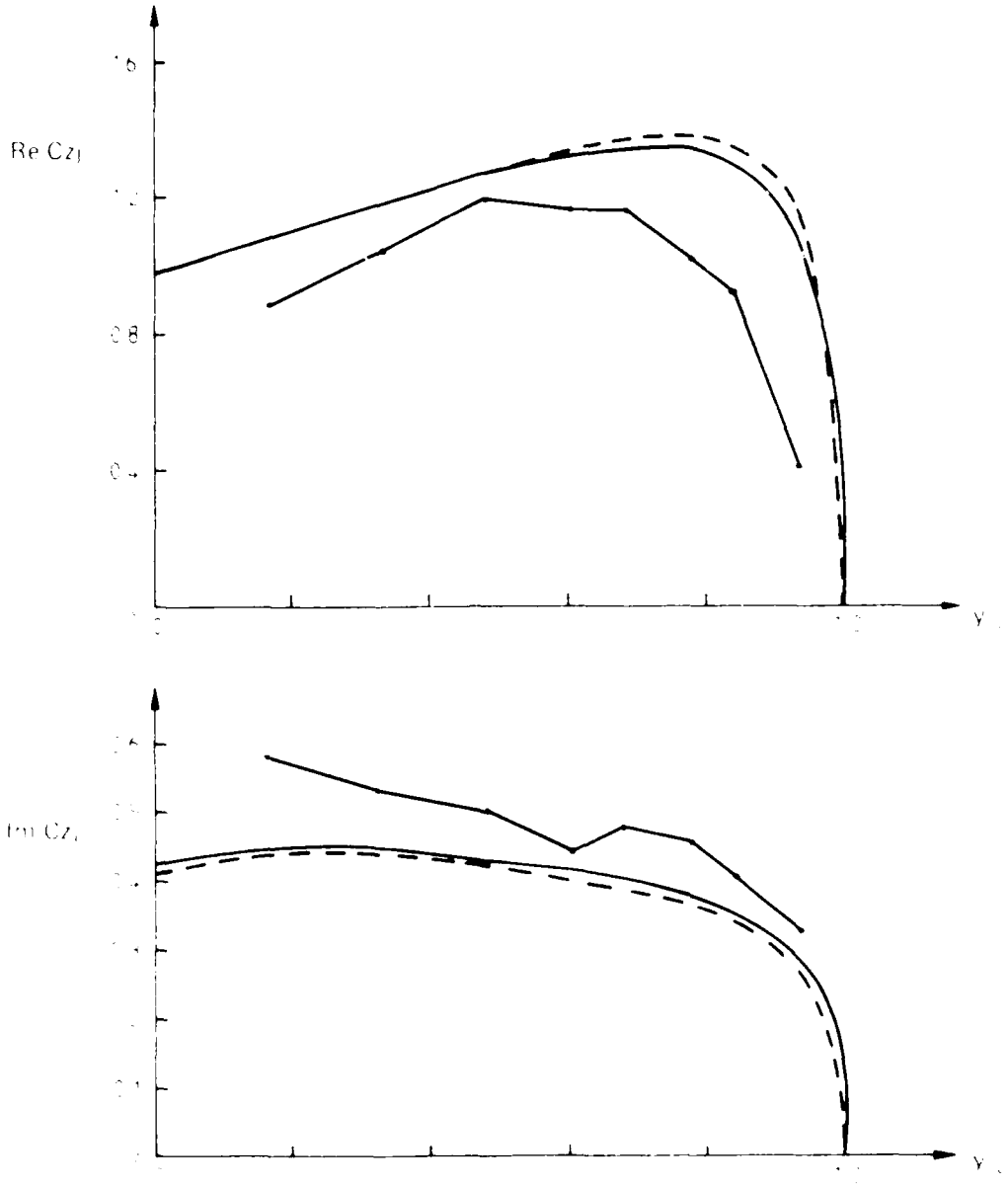

FIG. 13 UNSTEADY SPANWISE NORMAL FORCE DISTRIBUTION FOR THE CLEAN NLR WING AT M = 0.6 AND F = 40HZ.

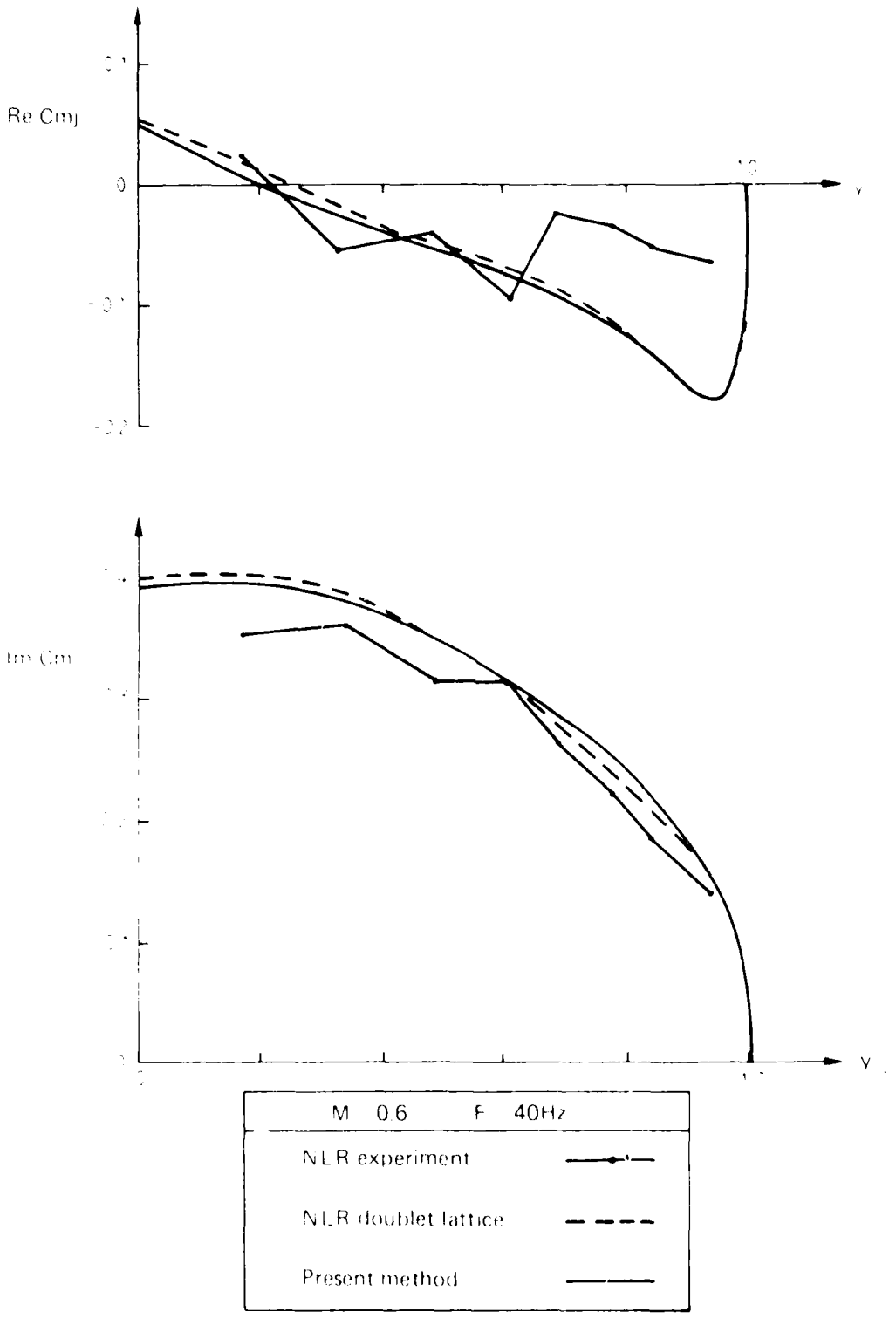

FIG. 14 UNSTEADY SPANWISE PITCHING MOMENT DISTRIBUTION FOR THE CLEAN NLR WING AT M = 0.6 AND F = 40HZ.

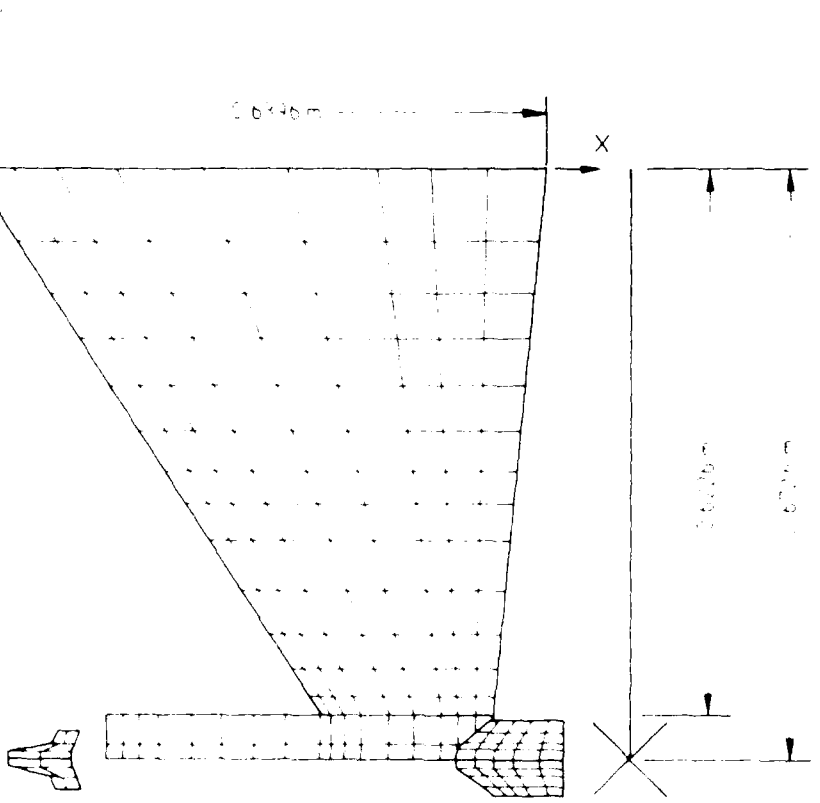

Number of panels	
Wing	117
Canard fins	24
Aft wings	80
Launcher + missile body	34
Total	255

Fig. 15 PANEL DISTRIBUTION FOR THE NLR WING WITH TIPSTORE CONFIGURATION USED IN CALCULATIONS WITH THE DOUBLET LATTICE METHOD.

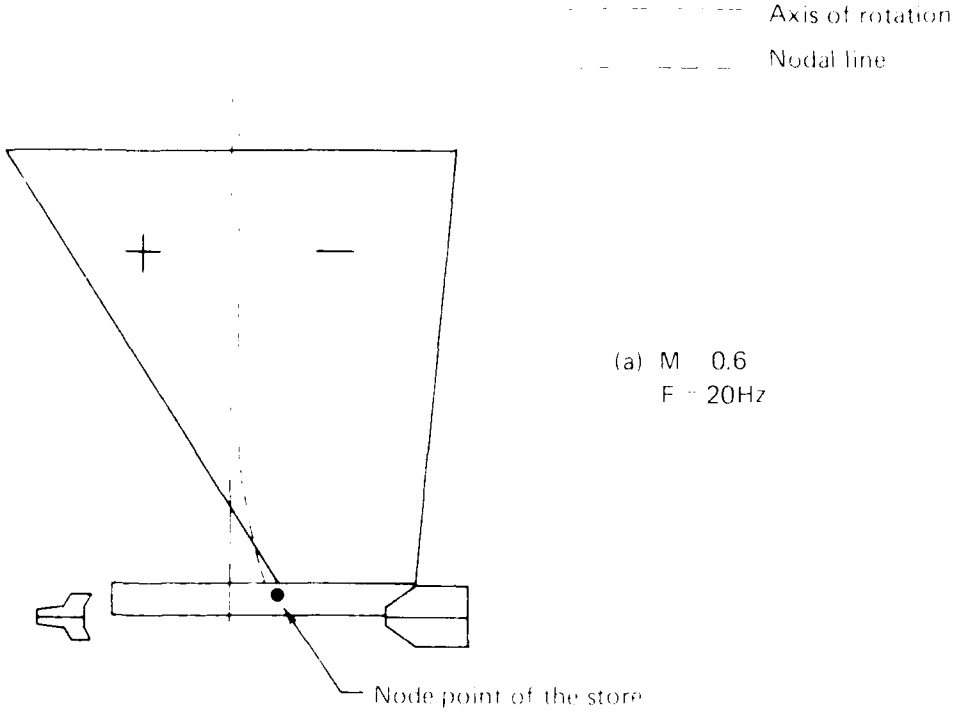

(a) M = 0.6
F = 20Hz

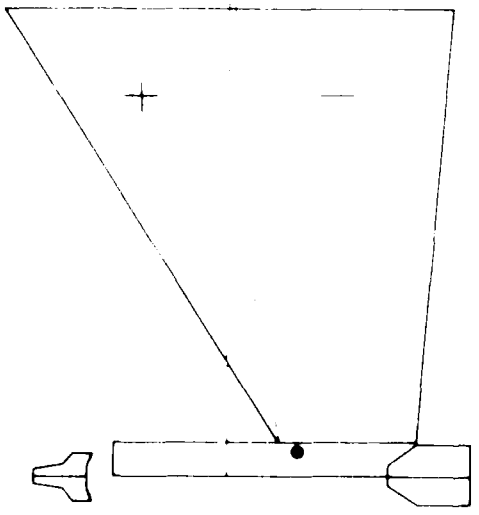

(b) M = 0.8
F = 20Hz

FIG. 16 IN-WIND VIBRATION MODES OF THE NLR WING WITH COMPLETE TIPSTORE

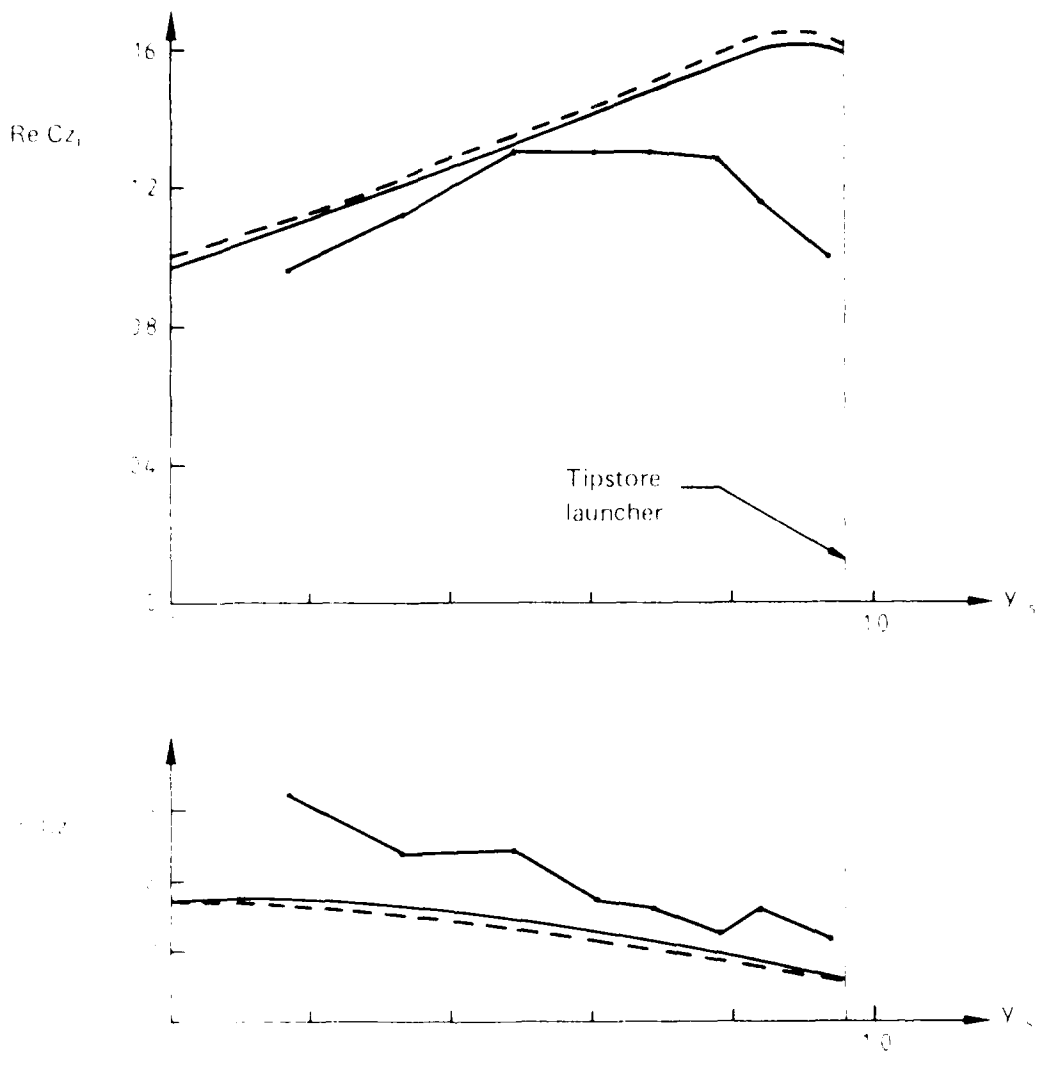

M 0.6 F 20 Hz	
NLR experiment	
NLR doublet lattice	
Present method	

SPANWISE NORMAL LOAD DISTRIBUTION FOR THE NLR
COMPLETE TIPSTORE AT M 0.6 AND F 20HZ

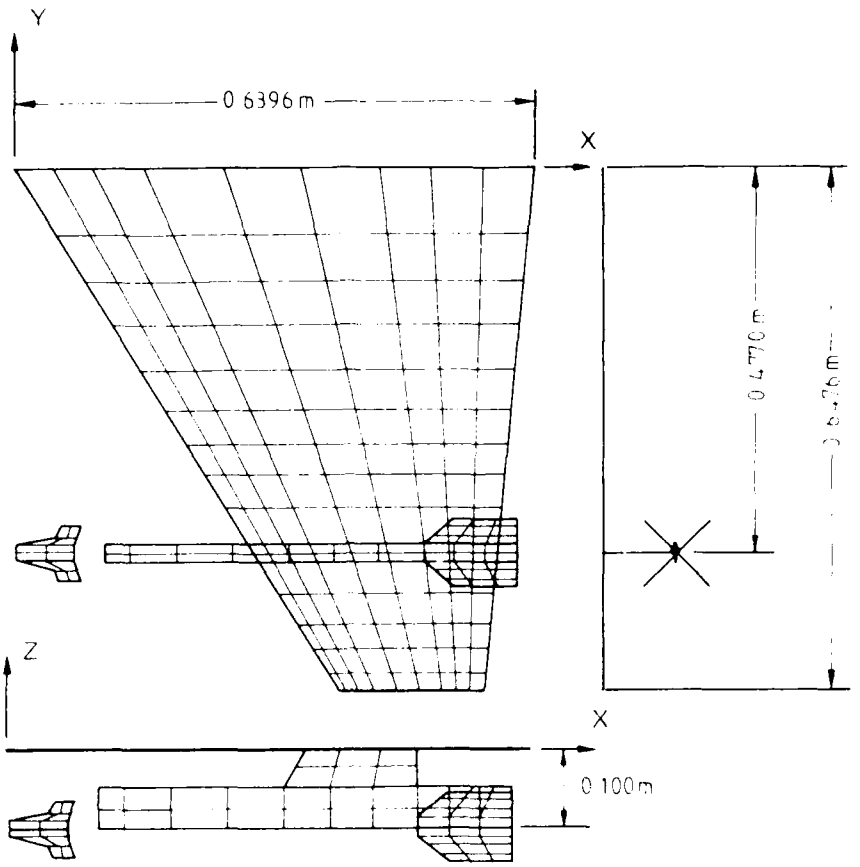

Number of panels	
Wing	126
Pylon	6
Canard fins	24
Aft wings	48
Launcher	20
Missile body	20
Total	244

FIG. 18 PANEL DISTRIBUTION FOR THE NLR WING WITH PYLON STORE USED IN THEORETICAL CALCULATIONS WITH THE DOUBLET LATTICE METHOD.

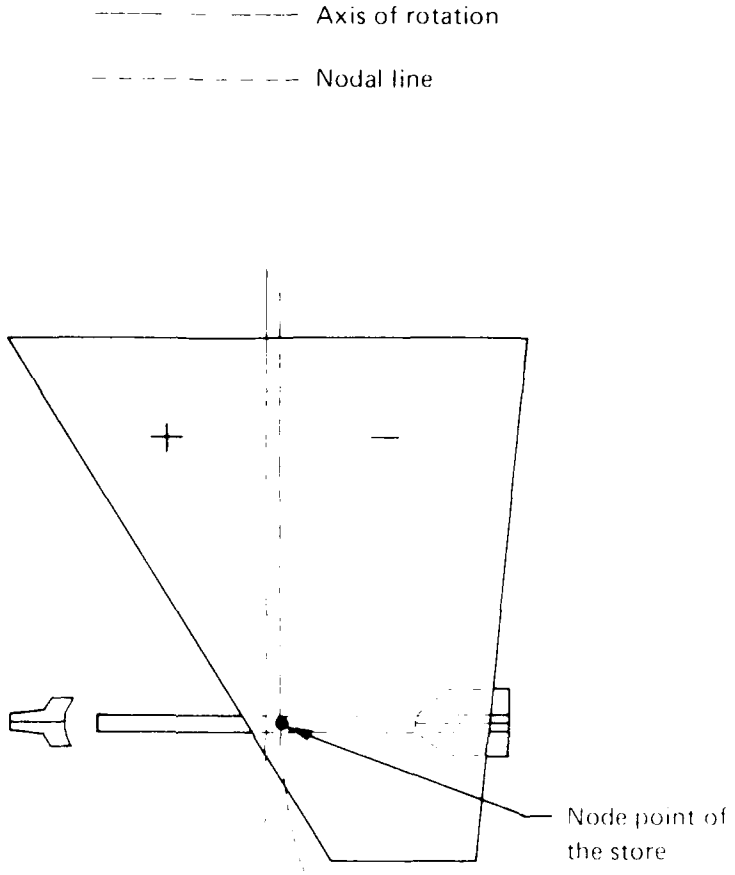

M 0.6 F - 20Hz

FIG. 19 IN WIND VIBRATION MODE OF THE NLR WING WITH PYLON AND COMPLETE UNDERWING STORE

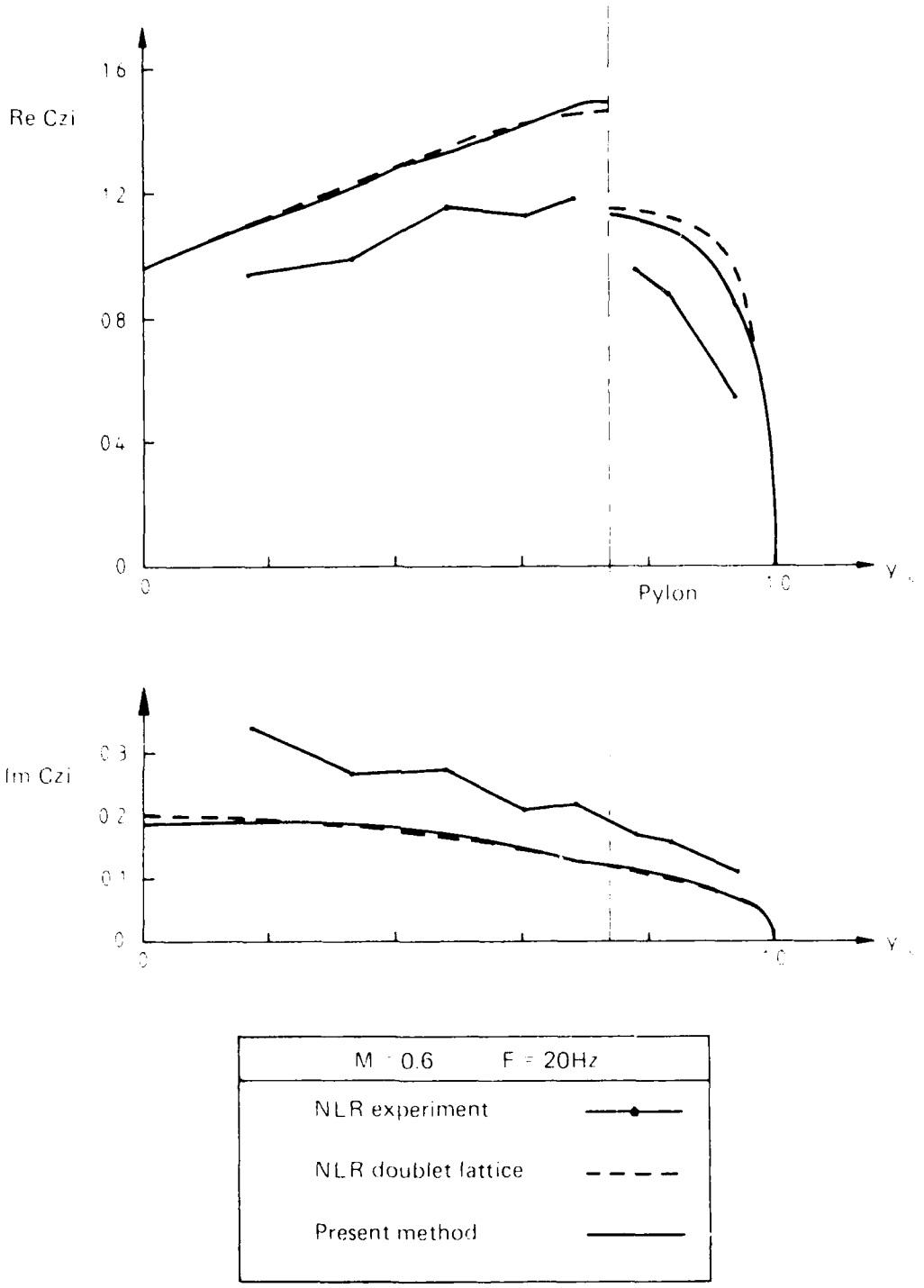

FIG. 20 UNSTEADY SPANWISE NORMAL FORCE DISTRIBUTIONS FOR THE NLR WING WITH COMPLETE PYLON AND STORE AT M = 0.6 AND F = 20HZ.

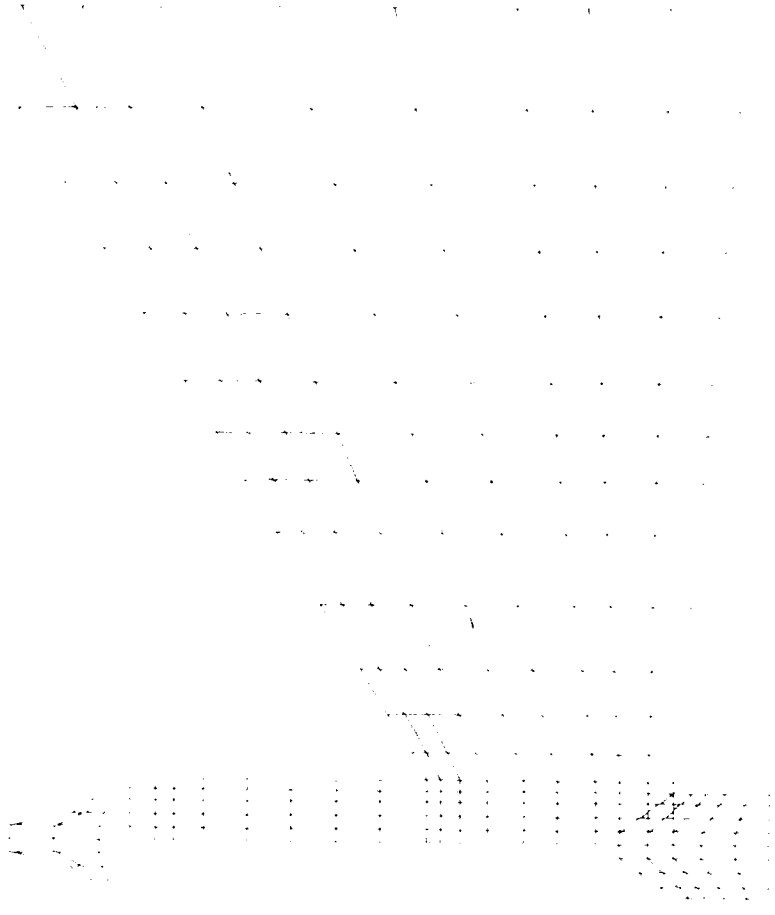

Number of panels	
Wing	112
Canard fins	24
Aft wings	80
Cannister + missile body	92
Total	308

FIG. 21 ALIGNED PANEL DISTRIBUTION FOR THE NEW WING W... FIPSTORE USED IN CALCULATIONS WITH THE PRESENT METHOD

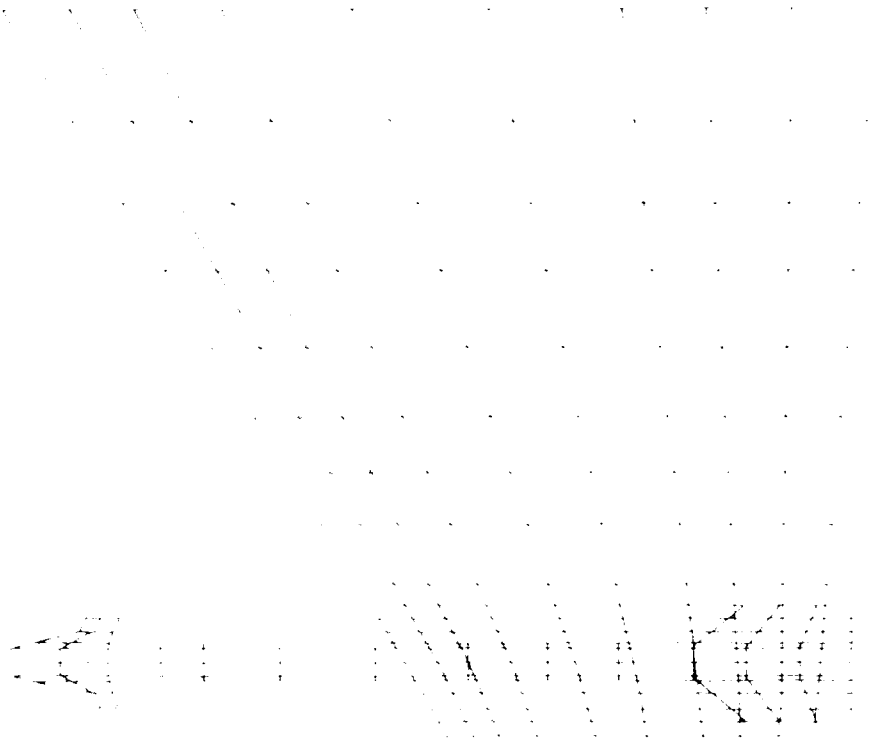

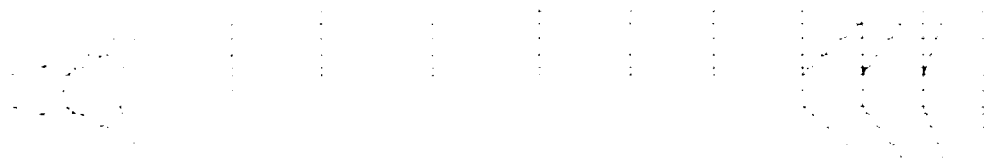

DISTRIBUTION

AUSTRALIA

DEPARTMENT OF DEFENCE

Defence Central

Chief Defence Scientist
Deputy Chief Defence Scientist (shared copy)
Superintendent, Science and Program Administration (shared copy)
Controller, External Relations, Projects & Analytical Studies (shared copy)
Counsellor, Defence Science, London (Doc. Data sheet only)
Counsellor, Defence Science, Washington (Doc. Data sheet only)
Defence Science Representative (Bangkok)
Defence Central Library
Document Exchange Centre, DISB (18 copies)
Joint Intelligence Organisation
Librarian H Block, Victoria Barracks, Melbourne
Director General—Army Development (NSO) (4 copies)

Aeronautical Research Laboratories

Director
Library
Divisional File--Structures
P. A. Farrell
I. Grundy
B. Emslie
N. Pollock
J. Lopez
M. Balick
Author: W. Waldman

Defence Research Centre

Library

Air Force Office

Air Force Scientific Adviser
Aircraft Research and Development Unit
    Scientific Flight Group
    Library
Technical Division Library

Government Aircraft Factories

Library
W. Baird, Aerodynamics
D. Scott
S. Georgiadis

DEPARTMENT OF AVIATION

Library

Statutory and State Authorities and Industry

Hawker de Havilland Victoria Limited, Library
Hawker de Havilland Aust. Pty Ltd, Bankstown, Library

Universities and Colleges

Melbourne
Engineering Library

Monash
Hargrave Library

Sydney
Engineering Library

N.S.W.
Physical Sciences Library
Library, Australian Defence Force Academy

Queensland
Library

RMIT
Library
Mr I. Herszberg, Civil & Aero Engineering Department
Dr L. Wood, Civil & Aero Engineering Department
Dr G. Fitz-Gerald, Mathematics Department
Dr J. Gear, Mathematics Department

CANADA

International Civil Aviation Organization, Library
NRC
Aeronautical & Mechanical Engineering Library

Universities and Colleges

Toronto
Institute for Aerospace Studies

FRANCE

ONERA, Library

GERMANY

Fachinformationszentrum Energie, Physik, Mathematik GMBH

INDIA

CAARC Coordinator Structures
Defence Ministry, Aero Development Establishment, Library
Hindustan Aeronautics Ltd, Library
National Aeronautical Laboratory, Information Centre

ISRAEL

Technion-Israel Institute of Technology
Professor J. Singer

ITALY

Professor Ing. Giuseppe Gabrielli

JAPAN

National Aerospace Laboratory
Institute of Space and Astronautical Science, Library

NETHERLANDS

National Aerospace Laboratory (NLR), Library

NEW ZEALAND

Defence Scientific Establishment, Library

SWEDEN

Aeronautical Research Institute, Library
Swedish National Defence Research Institute (FOA)

SWITZERLAND

Armament Technology and Procurement Group
F + W (Swiss Federal Aircraft Factory)

UNITED KINGDOM

CAARC, Secretary
Royal Aircraft Establishment
Bedford, Library
Farnborough, Dr D. E. Davies
CAARC Co-ordinator, Structures
Aircraft Research Association, Library
British Aerospace
Kingston-upon-Thames, Library
Hatfield-Chester Division, Library
Short Brothers Ltd, Technical Library

Universities and Colleges

London
Professor G. J. Hancock, Aero Engineering

Manchester
Professor, Applied Mathematics
Professor N. Johannesen, Fluid Mechanics

Liverpool
Fluid Mechanics Division, Dr J. C. Cummings

Cranfield Inst. of Technology
Library

Imperial College
Aeronautics Library

UNITED STATES OF AMERICA

NASA Scientific and Technical Information Facility
Boeing Company
Mr W. E. Binz
Mr J. C. McMillan
Lockheed-California Company
Lockheed Missiles and Space Company
Lockheed Georgia
McDonnell Aircraft Company, Library

Spares (10 copies)

Total (111 copies)

Department of Defence

DOCUMENT CONTROL DATA

1 a AR No	1 b Establishment No.	2 Document Date	3 Task No
AR-004-497	ARL-STRUC-R-423	August 1986	DST 82/053

4 Title	5 Security	6 No Pages
AN IMPROVED COMPUTATIONAL PROCEDURE FOR THE UNSTEADY DOUBLET LATTICE METHOD	a document: Unclassified b title: U. c abstract: U.	37 7 No Refs: 15

8 Author(s)	9 Downgrading Instructions
W. Waldman	—

10 Corporate Author and Address	11 Authority (*as appropriate*)
Aeronautical Research Laboratories, P.O. Box 4331, Melbourne, Victoria, 3001	a Sponsor c Downgrading b Security d Approval

12 Secondary Distribution (*of this document*)

Approved for public release

Overseas enquirers outside stated limitations should be referred through ASDIS, Defence Information Services Branch, Department of Defence, Campbell Park, CANBERRA, ACT, 2601

13 a This document may be ANNOUNCED in catalogues and awareness services available to

No limitations

13 b Citation for other purposes (*i.e. casual announcement*) may be (*select*) unrestricted (~~or as for 13 a~~)

14 Descriptors		15 COSATI Group
Unsteady flow	Lifting surfaces	01010
Aerodynamic loads	Computational fluid dynamics	

16 Abstract

A further modification and enhancement of the doublet lattice computational procedure in use at ARL is described. The theoretical basis for the new procedures used to integrate the unsteady Kernel function is covered in detail. A number of cases involving coplanar and non-parallel lifting surface combinations are studied, and the results are compared with those of other workers. These show generally good agreement, although the predictions of the magnitudes of the forces acting on a tipstore and an underwing store do not compare as favourably. The present method has been implemented at ARL into the FORTRAN 77 program called DOUBLAT.

This page is to be used to record information which is required by the Establishment for its own use but which will not be added to the DISTIS data base unless specifically requested.

16. Abstract (*Contd*)

17. Imprint

Aeronautical Research Laboratories, Melbourne

18. Document Series and Number	19. Cost Code	20. Type of Report and Period Covered
Structures Report 423	23 6925	

21. Computer Programs Used

22. Establishment File Ref(s)

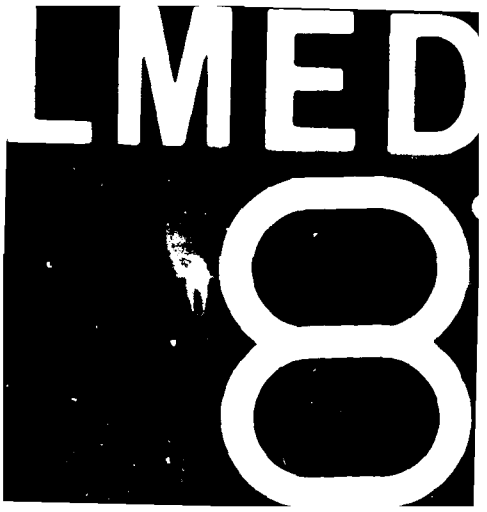
LMED
8